PL-TR-97-2031

SURFACE WAVE WAVEFORM INVERSION USING GDSF THEORY

R. B. Herrmann

Department of Earth and Atmospheric Sciences
St. Louis University
3507 Laclede Avenue
St. Louis, MO 63103

28 June 1996

Scientific Report No. 1

DEPARTMENT OF ENERGY
Office of Non-Proliferation
   and National Security
WASHINGTON, DC   20585

19980819 091

PHILLIPS LABORATORY
Directorate of Geophysics
AIR FORCE MATERIEL COMMAND
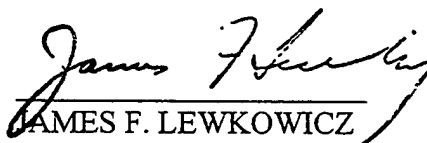**HANSCOM AFB, MA 01731-3010**

DTIC QUALITY INSPECTED 1

The views and conclusions contained in this document are those of the authors and should not be interpreted as representing the official policies, either express or implied, of the Air Force or U.S. Government.

This technical report has been reviewed and is approved for publication.

This report has been reviewed by the ESD Public Affairs Office (PA) and is releasable to the National Technical Information Service (NTIS).

Qualified requestors may obtain copies from the Defense Technical Information Center. All others should apply to the National Technical Information Service.

If your address has changed, or you wish to be removed from the mailing list, or if the addressee is no longer employed by your organization, please notify PL/IM, 29 Randolph Road, Hanscom AFB, MA 01731-3010. This will assist us in maintaining a current mailing list.

Do not return copies of this report unless contractual obligations or notices on a specific document requires that it be returned.

REPORT DOCUMENTATION PAGE

1. AGENCY USE ONLY *(Leave Blank)*	2. REPORT DATE 28 June 1996	3. REPORT TYPE AND DATES COVERED Scientific Report No. 1

4. TITLE AND SUBTITLE

Surface Wave Waveform Inversion Using GDSF Theory

6. AUTHORS

R.B. Herrmann

5. FUNDING NUMBERS
Contract No:
F19628-95-K-0019
PE 69120H
PR DENN
TA GM
WU AJ

7. PERFORMING ORGANIZATION NAME(S) AND ADDRESS(ES)
Department of Earth and Atmospheric Sciences
Saint Louis University
3507 Laclede Avenue
St. Louis, MO 63103

8. PERFORMING ORGANIZATION REPORT NUMBER

9. SPONSORING / MONITORING AGENCY NAME(S) AND ADDRESS(ES)
Phillips Laboratory
29 Randolph Road
Hanscom AFB, MA 01731-3010
Contract Manager: Delaine Reiter/GPE

10. SPONSORING / MONITORING AGENCY REPORT NUMBER
PL-TR-97-2031

11. SUPPLEMENTARY NOTES

12a. DISTRIBUTION / AVAILABILITY STATEMENT

12b. DISTRIBUTION CODE

13. ABSTRACT *(Maximum 200 words)*

The use of regionally recorded Rayleigh waves to estimate isotropic moment and psi-infinity for the purpose of yield estimation is investigated. These seismological parameters and their variability are consistent with other investigations. Psi-infinity shows less variability than isotropic moment as a yield estimator. Preliminary results on wave propagation in the Korean peninsula are also presented.

14. SUBJECT TERMS
Isotropic moment - yield, nuclear explosion, chemical explosion, seismic attenuation

15. NUMBER OF PAGES

16. PRICE CODE

17. SECURITY CLASSIFICATION OF REPORT	18. SECURITY CLASSIFICATION OF THIS PAGE	19. SECURITY CLASSIFICATION OF ABSTRACT	20. LIMITATION OF ABSTRACT
Unclassified	Unclassified	Unclassified	SAR

TABLE OF CONTENTS

This page left blank

Summary

This report consists of a review of the interpretation of Generalized Seismological Data Functionals (GSDF) as a means of refining earth structure through waveform modeling. An inversion procedure is developed, and examples are shown for synthetic and observed data.

The focus has been on the algorithm implementation, and more work must be done to understand the limitations and applicability of the technique with respect to real data. The effects poorly constrained source depth and mechanism as well as noisy data remain to be investigated. A useful tool has been implemented, though.

This page left blank

SURFACE WAVE WAVEFORM INVERSION USING GSDF THEORY

Tao-Ming Chang and Robert B. Herrmann

1. Introduction

In this report, we extend the Generalized Seismological Data Functionals (GSDF) theory to the inversion of broadband waveforms modeled as a superposition of surface-wave modes. We demonstrate the utility of this inversion algorithm by conducting a simple synthetic test, and then apply the algorithm to real data to see what new knowledge about earth structure can be obtained from this new inversion algorithm.

2. Theory of Generalized Seismological Data Functionals

Gee and Jordan (1992) introduced the theory of Generalized Seismological Data Functionals (GSDF) as a means of characterizing differences between observed and predicted seismograms in terms of *time delays* with respect to the earth model used. The importance of the Gee and Jordan (1992) paper is that it defines the framework for working with multimode signals.

To use the GSDF approach, we need to construct a synthetic seismogram ($\tilde{s}$), an isolation function ($\tilde{f}$) and single-mode seismograms. An isolation function is a sum of single-mode seismograms which may represent the dominant part of the observed seismogram (s). Using a cross-correlation technique, we can quantify the similarity observed and synthetic seismograms. For a model which does not significantly deviate from actual earth structure, the peak of cross-correlagrams will be located near zero lag-time for all frequency bands and for all windowed segments of the seismograms. The cross-correlagrams reflect the degree that the model used to create synthetic seismogram, isolation function and single-mode seismograms is different from real earth structure. To utilize this information, we have to extract information from different frequency ranges and interpret it in term of differences in earth structure.

Gee and Jordan (1992) call the extracted information Generalized Seismological Data Functionals (GSDF). In the following, we give a brief review of how the GSDF is defined, how the GSDF is related to familiar physical quantities, and how we extend this theory to invert for Earth structure Equations directly adapted from Gee and Jordan (1992) will be cited as (GJ.#), where # indicates the original equation number in their paper.

First, we review the definition and computation of a GSDF. We can use a Gaussian wavelet to approximate the filtered and windowed cross-correlagrams at a specified frequency. Specifically, the windowed, filtered cross-correlagram of an isolation function with a seismogram (either observed or synthetic) is modeled using a five-parameter Gaussian wavelet:

$$\mathbf{F}_i \mathbf{W} \mathbf{C}_{fs}(t) \approx g(t) \equiv A \, \mathrm{Ga}[\sigma_s(t - t_g)] \cos[\omega_s(t - t_p)] \qquad \text{(GJ.5)}$$

$$\mathbf{F}_i \mathbf{W} \tilde{\mathbf{C}}_{fs}(t) \approx \tilde{g}(t) \equiv \tilde{A} \, \mathrm{Ga}[\tilde{\sigma}_s(t - \tilde{t}_g)] \cos[\tilde{\omega}_s(t - \tilde{t}_p)] \qquad \text{(GJ.8)}$$

$$\mathbf{F}_i \mathbf{W} \tilde{\mathbf{C}}_{ff}(t) \equiv \mathrm{Ga}[\tilde{\sigma}_f t] \cos[\tilde{\omega}_f t]$$

where

$\mathbf{F}_i$ is a Gaussian frequency content filter with center frequency ω_i and half-bandwidth σ_i,

$\mathbf{W} = \mathrm{Ga}[\sigma_w(t - t_w)]\left\{1 + 0.01[\sigma_w(t - t_w)]^4 - \cdots\right\}$ is a temporal window with half-bandwidth σ_w and centered at t_w; usually $t_w = t_c$, where t_c is the lag-time of the peak of $\mathbf{F}_i \mathbf{W} \mathbf{C}_{ff}$,

$\mathbf{C}_{fs}(t) \equiv \tilde{f}(t) \otimes s(t)$, $\otimes$ represents cross-correlation, is the cross-correlation with the observed time history,

$\tilde{\mathbf{C}}_{fs}(t) \equiv \tilde{f}(t) \otimes \tilde{s}(t)$, is the cross-correlation with the synthetic time history,

$\mathrm{Ga}[x] \equiv \exp(-\dfrac{x^2}{2})$, Ga is the Gaussian function,

A is the amplitude of Gaussian envelope,

σ is the half-bandwidth of envelope spectrum,

ω is the angular frequency of oscillating wavelet,

t_g is the envelope group delay from zero lag-time,

t_p is the wavelet phase delay from zero lag-time,

the subscript s denotes observed seismogram, subscript s combined with $\sim$ denotes synthetic seismogram, and the subscript f with $\sim$ denotes isolation filter.

From (GJ.5) and (GJ.8), Gee and Jordan define four data functionals to characterize the agreement between observed and predicted time histories:

$$\delta t_p = t_p - \tilde{t}_p \qquad\qquad (GJ.9)$$

$$\delta t_g = t_g - \tilde{t}_g \qquad\qquad (GJ.10)$$

$$\delta t_q = -\frac{1}{\tilde{\omega}_s} [\ln A - \ln \tilde{A}] \qquad\qquad (GJ.11)$$

$$\delta t_a = -\frac{1}{\tilde{\sigma}_s^2} [\omega_s - \tilde{\omega}_s] \qquad\qquad (GJ.12)$$

These four data functionals are related to differential phase delay, differential group delay, differences in logarithmic amplitudes and the differences in center frequencies. These four data functionals are defined from two filtered, windowed cross-correlagrams, they can be transformed into the more familiar quantities such as phase velocity, group velocity, and attenuation corrections.

We will briefly describe this transformation. We note that all filtered and windowed cross-correlagrams will be normalized by scaling $\mathbf{F}_i \mathbf{W} \tilde{\mathbf{C}}_{ff}$ to unit amplitude. Also, if the observed and synthetic seismograms are composed only of a single mode, then the GSDF are easily interpreted in terms of differences in modeled and actual phase velocity, group velocity and Q. For multi-mode time histories their interpretation is much more difficult.

Before relating GSDF to physical quantities, we must know the roles these quantities play in wave propagation. For a known instrument response and source, the difference between the spectrum of isolation filter

$\tilde{f}(\omega) = I(\omega)\tilde{P}(\omega)S(\omega)$ and its corresponding component of the observed seismograms $f(\omega) = I(\omega)P(\omega)S(\omega)$ is called "differential propagation". The are related by the equation

$$f(\omega) = \frac{P(\omega)}{\tilde{P}(\omega)}\tilde{f}(\omega)$$

$$= D(\omega)\tilde{f}(\omega) \tag{GJ.42}$$

$$= e^{i\delta k(\omega)R}\tilde{f}(\omega) = e^{i[k(\omega)-\tilde{k}(\omega)]R}\tilde{f}(\omega)$$

where R is source-receiver distance. To a first order approximation, the differential propagation can be approximated as

$$D(\omega) \approx \exp\left(-\omega_j\delta\tau_q(\omega_j) - (\omega - \omega_j)\delta\tau_a(\omega_j)\right) \tag{GJ.44}$$

$$+ \exp\left(i\left[\omega_j\delta\tau_p(\omega_j) + (\omega - \omega_j)\delta\tau_q(\omega_j)\right]\right)$$

The propagation effects of the isolation filter $\tilde{f}(t)$ and the corresponding waveform $f(t)$ on the observed seismogram are defined in four equations which are described in terms of familiar physical quantities such as total phase delay, total group delay, and attenuation factor.

$$\delta\tau_p(\omega_j) \equiv \tau_p(\omega_j) - \tilde{\tau}_p(\omega_j) \tag{GJ.45}$$

$$\delta\tau_g(\omega_j) \equiv \tau_g(\omega_j) - \tilde{\tau}_g(\omega_j) \tag{GJ.46}$$

$$\delta\tau_q(\omega_j) \equiv \frac{1}{2}\tilde{\tau}_p(\omega_j)[Q^{-1} - \tilde{Q}^{-1}] \tag{GJ.47}$$

$$\delta\tau_a(\omega_j) \equiv \frac{1}{2}\tilde{\tau}_g(\omega_j)[Q^{-1} - \tilde{Q}^{-1}] \tag{GJ.48}$$

where

$\tau_p(\omega_j)$ is total phase delay of $f(t)$ at an arbitrary frequency ω_j with respect to the original time,

$\tilde{\tau}_p(\omega_j)$ is total phase delay of $\tilde{f}(t)$ at ω_j,

4

$\tau_g(\omega_j)$ is total group delay of $f(t)$ at ω_j,

$\tilde{\tau}_g(\omega_j)$ is total group delay of $\tilde{f}(t)$ at ω_j,

Q is attenuation factor of $f(t)$,

$\tilde{Q}^{-1}$ is attenuation factor of $\tilde{f}(t)$.

This means that whenever we are able to measure four differential quantities $\delta\tau_x$ from observed and synthetic seismograms at a certain frequency ω_j, we can approximate the true waveform spectrum behavior $f(\omega)$ at any arbitrary frequency ω to a first order precision.

The GSDF δt_x based on the filtered, windowed cross-correlation, and the $\delta\tau_x$ is related to the time domain windowing function. Their relationships are given by

$$\delta t_g \approx \delta\tau_g(\tilde{\omega}_f) + (1 - \xi_1^2)[t_c - \delta\tau_g(\tilde{\omega}_f)] \qquad \text{(GJ.56)}$$

$$\delta t_p \approx \delta\tau_p(\tilde{\omega}_f) + (1 - \xi_1^2)(\frac{\tilde{\omega}_f - \tilde{\omega}_c}{\tilde{\omega}_f})[t_c - \delta\tau_g(\tilde{\omega}_f)] \qquad \text{(GJ.57)}$$

$$\delta t_a \approx \xi_1^2 \delta\tau_a(\tilde{\omega}_f) \qquad \text{(GJ.58)}$$

$$\delta t_q \approx \delta\tau_q(\tilde{\omega}_f) - (1 - \xi_1^2)(\frac{\tilde{\omega}_f - \tilde{\omega}_c}{\tilde{\omega}_f})\delta\tau_a(\tilde{\omega}_f) \qquad \text{(GJ.59)}$$

where

$\tilde{\omega}_c$ is the frequency from $\tilde{\mathbf{C}}_{ff}$,

ξ_1 is a window width factor,

t_c is the lag-time of the peak of cross-correlagram $\mathbf{F}_i\mathbf{WC}_{ff}$.

There is an additional assumption that must be stated. Due to the difficulty in relating the isolation filter's corresponding feature in observed seismogram, it is not easy to evaluate $\mathbf{F}_i\mathbf{WC}_{ff}$. However, if the windowing procedure is effective in isolating $f(t)$ from other phases on the seismograms, then $\mathbf{F}_i\mathbf{WC}_{fs} \approx \mathbf{F}_i\mathbf{WC}_{ff}$.

We can estimate t_c from an isolated waveform. For non-isolated waveforms, the $\mathbf{C}_{ff}$ can not be simply replaced by $\mathbf{C}_{fs}$ and this is a more general

situation. For non-isolated waveforms, the Gaussian wavelet can be represented as a sum of interference effects of different modes.

$$\mathbf{F}_i\mathbf{W}\tilde{\mathbf{C}}_{fs}(t) = \sum_{m=1}^{N}\sum_{n=1}^{N}\mathbf{F}_i\mathbf{W}\tilde{\mathbf{C}}_{mn}(t) \qquad\qquad \text{(GJ.63)}$$

$$\mathbf{F}_i\mathbf{W}\mathbf{C}_{fs}(t) = \sum_{m=1}^{N}\sum_{n=1}^{N}\mathbf{F}_i\mathbf{W}\mathbf{C}_{mn}(t)$$

where

$$\mathbf{C}_{mn}(t) \equiv [mode\ m\ of\ \tilde{f}(t)] \boxtimes [mode\ n\ of\ f(t)],$$

$$\tilde{\mathbf{C}}_{mn}(t) \equiv [mode\ m\ of\ \tilde{f}(t)] \boxtimes [\ mode\ n\ of\ \tilde{f}(t)].$$

We now characterize these by the relation

$$\mathbf{F}_i\mathbf{W}\tilde{\mathbf{C}}_{mn}(t) \approx \tilde{A}_{mn}\mathrm{Ga}[\tilde{\sigma}_f(t - \tilde{t}_g^{mn})]\cos[\tilde{\omega}_{mn}(t - \tilde{t}_p^{mn})] \qquad \text{(GJ.68)}$$

where

$$\tilde{A}_{mn} \equiv exp(-\tilde{\omega}_f\tilde{t}_q^{mn}),$$

$$\tilde{\omega}_{mn} \equiv \tilde{\omega}_f - \tilde{\sigma}_f\tilde{t}_a^{mn}.$$

In this case, we need to know four time shifts that describe the deviations of $\mathbf{F}_i\mathbf{W}\tilde{\mathbf{C}}_{fs}$ from $\mathbf{F}_i\mathbf{W}\tilde{\mathbf{C}}_{ff}$. Assume that the windowing and filtering effectively suppress the bandwidth variations, so that $\tilde{\sigma}_s \approx \tilde{\sigma}_f$. The four time shifts are the phase delay $\tilde{t}_p$, a group delay $\tilde{t}_g$, and two amplitude parameters

$$\tilde{t}_q = -\frac{1}{\tilde{\omega}_f}\ln\tilde{A} \qquad\qquad \text{(GJ.60)}$$

$$\tilde{t}_a = -\frac{1}{\tilde{\sigma}_f^2}[\tilde{\omega}_s - \tilde{\omega}_f] \qquad\qquad \text{(GJ.61)}$$

By defining the following notation,

$$B_{mn} = \frac{1}{2\pi_{1/2}}\exp[-\tilde{\omega}_f(\tilde{t}_q^{mn} - \tilde{t}_q)]\mathrm{Ga}[\tilde{\sigma}_f(\tilde{t}_g^{mn} - \tilde{t}_g)] \qquad \text{(GJ.73)}$$

$$\phi_{mn} = (\tilde{\omega}_f - \tilde{\sigma}_f^2\tilde{t}_a^{mm})(\tilde{t}_p^{mn} - \tilde{t}_p) - \tilde{\sigma}_f^2(\tilde{t}_a^{mn} - \tilde{t}_a)(\tilde{t}_p - \tilde{t}_g) \qquad \text{(GJ.74)}$$

the perturbation expansions can be simplified by using a set $N \times N$ matrices

$$(\mathbf{C})_{mn} = B_{mn}\cos\phi_{mn} \qquad\qquad \text{(GJ.75)}$$

6

$$(\mathbf{S})_{mn} = B_{mn}\sin\phi_{mn} \tag{GJ.76}$$

$$(\mathbf{C_x})_{mn} = B_{mn}\tilde{\omega}_f(\tilde{t}_x^{mn} - \tilde{t}_x)cos\phi_{mn} \tag{GJ.77}$$

$$(\mathbf{S_x})_{mn} = B_{mn}\tilde{\omega}_f(\tilde{t}_x^{mn} - \tilde{t}_x)sin\phi_{mn} \tag{GJ.78}$$

Gee and Jordan (1992) gave the following linearized relationships between the GSDFs and computable quantities from individual mode branches.

$$\delta t_q = 1\cdot\mathbf{C}\cdot\delta\mathbf{t_q} + 1\cdot\mathbf{S}\cdot\delta\mathbf{t_p} \tag{GJ.84}$$

$$\delta t_p = -1\cdot\mathbf{S}\cdot\delta\mathbf{t_q} + 1\cdot\mathbf{C}\cdot\delta\mathbf{t_p} \tag{GJ.85}$$

$$\delta t_a = -1\cdot(\mathbf{C_a}+\mathbf{S_g})\cdot\delta\mathbf{t_q} + 1\cdot(\mathbf{C_g}-\mathbf{S_a})\cdot\delta\mathbf{t_p} + 1\cdot\mathbf{C}\cdot\delta\mathbf{t_a} + 1\cdot\mathbf{S}\cdot\delta\mathbf{t_g} \tag{GJ.86}$$

$$\delta t_g = -1\cdot(\mathbf{C_g}-\mathbf{S_a})\cdot\delta\mathbf{t_q} - 1\cdot(\mathbf{C_a}+\mathbf{S_g})\cdot\delta\mathbf{t_p} - 1\cdot\mathbf{S}\cdot\delta\mathbf{t_a} + 1\cdot\mathbf{C}\cdot\delta\mathbf{t_g} \tag{GJ.87}$$

The $\mathbf{1}$ is a N-dimension vector, each element of which equals one. The $\delta\mathbf{t_x}$ is a N-vector whose n'th component is δt_x^n, the perturbation corresponding to the quantity x of n'th mode. In the following section, we will translate this $\delta\mathbf{t_x}$ into $\delta\tau_\mathbf{x}$ which directly relate to seismogram and has clear physical meaning.

3. Structure Inversion

To apply GSDF theory in structure inversion, we must construct the inversion kernel, $\mathbf{G}$ for our inversion. The inverse problem can be simply expressed in the form :

$$\delta\tau_\mathbf{x} = \mathbf{G_x}\cdot\delta\mathbf{m}$$

where

$\mathbf{x}$ indicates one of $\{\mathbf{p},\mathbf{g},\mathbf{q},\mathbf{a}\}$.

$\delta\tau_\mathbf{x}$ is an N-vector for corresponding to N modes,

$\mathbf{G_x}$ is an $N\times k$ Frechet kernel matrix for structural inverse problem,

$\delta\mathbf{m}$ is a model correction vector for k unknowns.

Keep in mind, that $\delta\tau_x$ is not measurable but fortunately GSDF theory provides a way to compute these nonmeasurable quantities using the mode

interference relationship. Thus, in actual application of GSDF theory, we must relate $\delta \tau_{\mathbf{x}}$ to $\delta \mathbf{t}_{\mathbf{x}}$ to create the kernel $\mathbf{G_x}$.

From (GJ.56-59), we can transform $\delta \tau_{\mathbf{x}}$ to $\delta \mathbf{t}_{\mathbf{x}}$ as

$$\delta \mathbf{t_g} = \delta \tau_{\mathbf{g}}(\tilde{\omega}_f) + (1 - \xi_1^2)[t_c \mathbf{1} - \delta \tau_{\mathbf{g}}(\tilde{\omega}_f)]$$

$$\delta \mathbf{t_p} = \delta \tau_{\mathbf{p}}(\tilde{\omega}_f) + a[t_c \mathbf{1} - \delta \tau_{\mathbf{g}}(\tilde{\omega}_f)]$$

$$\delta \mathbf{t_a} = \xi_1^2 \delta \tau_{\mathbf{a}}(\tilde{\omega}_f)$$

$$\delta \mathbf{t_q} = \delta \tau_{\mathbf{q}}(\tilde{\omega}_f) - a\delta \tau_{\mathbf{a}}(\tilde{\omega}_f)$$

where $a = (1 - \xi_1^2)(\dfrac{\tilde{\omega}_f - \tilde{\omega}_c}{\tilde{\omega}_f})$. Substituting these into (GJ.84-87) gives the following equations which relate the four GSDFs to inversion kernels $\mathbf{G_x}$.

$$\delta t_p = \mathbf{1} \cdot \mathbf{C} \cdot \mathbf{1} a\, t_c + \mathbf{1} \cdot \left[\mathbf{C}(\mathbf{G_p} - a\mathbf{G_g}) - \mathbf{S}(\mathbf{G_q} - a\mathbf{G_a}) \right] \delta \mathbf{m}$$

$$\delta t_q = \mathbf{1} \cdot \mathbf{S} \cdot \mathbf{1} a\, t_c + \mathbf{1} \cdot \left[\mathbf{C}(\mathbf{G_q} - a\mathbf{G_a}) + \mathbf{S}(\mathbf{G_p} - a\mathbf{G_g}) \right] \delta \mathbf{m}$$

$$\delta t_a = \mathbf{1} \cdot (\mathbf{C_g} - \mathbf{S_a}) \cdot \mathbf{1} a\, t_c + \mathbf{1} \cdot \mathbf{S} \cdot \mathbf{1}(1 - \xi_1^2)t_c$$

$$+ \mathbf{1} \cdot \left[-(\mathbf{C_a} + \mathbf{S_g})(\mathbf{G_q} - a\mathbf{G_a}) + (\mathbf{C_g} - \mathbf{S_a})(\mathbf{G_p} - a\mathbf{G_g}) + \xi_1^2 \mathbf{C} \mathbf{G_a} + \xi_1^2 \mathbf{S} \mathbf{G_g} \right] \delta \mathbf{m}$$

$$\delta t_g = -\mathbf{1} \cdot (\mathbf{C_a} + \mathbf{S_g}) \cdot \mathbf{1} a\, t_c + \mathbf{1} \cdot \mathbf{C} \cdot \mathbf{1}(1 - \xi_1^2)t_c$$

$$+ \mathbf{1}\left[-(\mathbf{C_g} - \mathbf{S_a})(\mathbf{G_q} - a\mathbf{G_a}) - (\mathbf{C_a} + \mathbf{S_g})(\mathbf{G_p} - a\mathbf{G_g}) - \xi_1^2 \mathbf{S} \mathbf{G_a} + \xi_1^2 \mathbf{C} \mathbf{G_g} \right] \delta \mathbf{m}$$

Now, we have a general form of inversion problem for earth structure in terms of the GSDF's δt_x, kernels $\mathbf{G_x}$, and the interference effects $\mathbf{C}, \mathbf{S}, \mathbf{C_x}, \mathbf{S_x}$.

At this point, it is possible to outline this structure inversion problem. At a particular frequency, according to GSDF theory, using cross-correlation technique we can obtain four measurements as our "observations" (GJ.9-12) and evaluate the mode interference, which we will use with $\mathbf{G_x}$ to form inversion kernels. Therefore, we perform this measuring procedure at several frequencies, we then have the "data vector" and "kernel matrix" ready for

inversion. In the following sections, we will show how we create the kernels $(\mathbf{G_x})$.

Kernel $\mathbf{G_p}$

Kernel $\mathbf{G_p}$ relates phase velocity changes to model perturbations.

$$\delta \tau_{\mathbf{p}} = \mathbf{G_p} \cdot \delta \mathbf{m}$$

The n'th component in the differential phase velocity vector $\delta \tau_{\mathbf{p}}$, $\delta \tau_{p_n}$ is define as

$$\delta \tau_{p_n} = \frac{R}{c_{n\,obs}} - \frac{R}{c_{n\,syn}}$$

$$= \frac{R}{c_n + \delta c_n} - \frac{R}{c_n} = \frac{R}{c_n}\left[-1 + (1 - \frac{\delta c_n}{c_n} + (\frac{\delta c_n}{c_n})^2 \cdots) \right]$$

$$= \frac{R}{c_n}\left[-\frac{\delta c_n}{c_n} + (\frac{\delta c_n}{c_n})^2 \cdots \right]$$

$$\approx -\frac{R}{c_n{}^2}\delta c_n = \left[-\frac{R}{c_n{}^2}\frac{\partial c_n}{\partial \mathbf{m}} \right]\cdot \delta \mathbf{m}$$

where

R is source-receiver distance,

c_n is phase velocity for n'th mode of synthetic seismogram.

In the matrix form, we can exactly see the meaning of $\delta \tau_{p_1}$ as the total phase delay for *mode* 1 when model $\mathbf{m}$ changes into $\mathbf{m} + \delta \mathbf{m}$.

$$
\begin{bmatrix} \delta \tau_{p_1} \\ \delta \tau_{p_2} \\ \cdot \\ \delta \tau_{p_N} \end{bmatrix}_{N \times 1}
= -
\begin{bmatrix}
\frac{R}{c_1^2}\frac{\partial c_1}{\partial m_1} & \frac{R}{c_1^2}\frac{\partial c_1}{\partial m_2} & \frac{R}{c_1^2}\frac{\partial c_1}{\partial m_3} & \cdots & (\#1\ mode) \\
\frac{R}{c_2^2}\frac{\partial c_2}{\partial m_1} & \frac{R}{c_2^2}\frac{\partial c_2}{\partial m_2} & \frac{R}{c_2^2}\frac{\partial c_2}{\partial m_3} & \cdots & (\#2\ mode) \\
\cdots & \cdots & \cdots & \cdots & \cdots \\
\frac{R}{c_N^2}\frac{\partial c_N}{\partial m_1} & \frac{R}{c_N^2}\frac{\partial c_N}{\partial m_2} & \frac{R}{c_N^2}\frac{\partial c_N}{\partial m_3} & \cdots & (\#N\ mode)
\end{bmatrix}_{N \times k}
\begin{bmatrix} \delta m_1 \\ \delta m_2 \\ \delta m_3 \\ \cdot \\ \cdot \\ \delta m_k \end{bmatrix}_{k \times 1}
$$

9

Kernel G_g

To construct kernel $\mathbf{G_g}$ which relates group velocity variation to model perturbations,

$$\delta \tau_{\mathbf{g}} = \mathbf{G_g} \cdot \delta \mathbf{m}$$

the n'th component in differential group velocity vector $\delta \tau_{\mathbf{g}}$, $\delta \tau_{g_n}$ is defined as

$$\delta \tau_{g_n} = \frac{R}{U_{n\,obs}} - \frac{R}{U_{n\,syn}}$$

$$= \frac{R}{U_n + \delta U_n} - \frac{R}{U_n} = \frac{R}{U_n} \left[-1 + (1 - \frac{\delta U_n}{U_n} + (\frac{\delta U_n}{U_n})^2 \cdots) \right]$$

$$= \frac{R}{U_n} \left[-\frac{\delta U_n}{U_n} + (\frac{\delta U_n}{U_n})^2 \cdots \right]$$

$$\approx -\frac{R}{U_n^2} \delta U_n = \left[-\frac{R}{U_n^2} \frac{\partial U_n}{\partial \mathbf{m}} \right] \cdot \delta \mathbf{m}$$

where

U_n is group velocity of n'th mode synthetic seismogram.

In matrix form

$$\begin{bmatrix} \delta \tau_{g_1} \\ \delta \tau_{g_2} \\ \cdot \\ \delta \tau_{g_N} \end{bmatrix}_{N \times 1} = - \begin{bmatrix} \dfrac{R}{U_1^2} \dfrac{\partial U_1}{\partial m_1} & \dfrac{R}{U_1^2} \dfrac{\partial U_1}{\partial m_2} & \dfrac{R}{U_1^2} \dfrac{\partial U_1}{\partial m_3} & \cdots & (\#1\ mode) \\ \dfrac{R}{U_2^2} \dfrac{\partial U_2}{\partial m_1} & \dfrac{R}{U_2^2} \dfrac{\partial U_2}{\partial m_2} & \dfrac{R}{U_2^2} \dfrac{\partial U_2}{\partial m_3} & \cdots & (\#2\ mode) \\ \cdots & \cdots & \cdots & \cdots & \cdots \\ \dfrac{R}{U_N^2} \dfrac{\partial U_N}{\partial m_1} & \dfrac{R}{U_N^2} \dfrac{\partial U_N}{\partial m_2} & \dfrac{R}{U_N^2} \dfrac{\partial U_N}{\partial m_3} & \cdots & (\#N\ mode) \end{bmatrix}_{N \times k} \begin{bmatrix} \delta m_1 \\ \delta m_2 \\ \delta m_3 \\ \cdot \\ \cdot \\ \delta m_k \end{bmatrix}_{k \times 1}$$

Kernel G_q

To create kernel $\mathbf{G_q}$ which relates attenuation to model perturbations,

$$\delta\tau_\mathbf{q} = \mathbf{G_q} \cdot \delta\mathbf{m}$$

we extend (GJ.47) into a general matrix form and reformulate the above equation to yield

$$\delta\tau_\mathbf{q} = \frac{1}{2}\,\tilde{\tau}_p(\omega)[Q^{-1} - \tilde{Q}^{-1}]$$

$$= \frac{1}{2}\left[\tilde{\tau}_p(\omega)\frac{\partial Q^{-1}}{\partial\mathbf{m}}\right]\delta\mathbf{m}$$

$$= \mathbf{G_q} \cdot \delta\mathbf{m}$$

Using the relationship between γ and Q, the partial derivative of γ with respect to model perturbations can be calculated.

$$\gamma_n = \frac{\omega}{2c_{0_n}}\,Q_n^{-1}$$

$$\frac{\partial\gamma_n}{\partial\mathbf{m}} = \frac{\omega}{2c_{0_n}}\frac{\partial Q_n^{-1}}{\partial\mathbf{m}} - Q_n^{-1}\frac{\omega}{2c_{0_n}{}^2}\frac{\partial c_{0_n}}{\partial\mathbf{m}}$$

Therefore, the partial derivative of Q_{RL}^{-1} can be rewritten as

$$\frac{\partial Q_n^{-1}}{\partial\mathbf{m}} = \left[\frac{\partial\gamma_n}{\partial\mathbf{m}} + Q_n^{-1}\frac{\omega}{2c_{0_n}}\frac{\partial c_{0_n}}{\partial\mathbf{m}}\right]\frac{2c_{0_n}}{\omega}$$

The n'th row (# n *mode*) of kernel $\mathbf{G_q}$ is

$$(\mathbf{G_q})_n = \tilde{\tau}_{p_n}(\omega)\left\{\frac{c_{0_n}}{\omega}\frac{\partial\gamma_n}{\partial\mathbf{m}} + \frac{Q_n^{-1}}{2c_{0_n}}\frac{\partial c_{0_n}}{\partial\mathbf{m}}\right\}$$

$\mathbf{G_q}$ in matrix form is

$$
\begin{bmatrix}
\tilde{\tau}_{p_1}\left(\dfrac{c_{0_1}}{\omega}\dfrac{\partial \gamma_1}{\partial m_1}+\dfrac{Q_1^{-1}}{2c_{0_1}}\dfrac{\partial c_{0_1}}{\partial m_1}\right) & \tilde{\tau}_{p_1}\left(\dfrac{c_{0_1}}{\omega}\dfrac{\partial \gamma_1}{\partial m_2}+\dfrac{Q_1^{-1}}{2c_{0_1}}\dfrac{\partial c_{0_1}}{\partial m_2}\right) & \cdots & (\#1\ mode) \\[2.5ex]
\tilde{\tau}_{p_2}\left(\dfrac{c_{0_2}}{\omega}\dfrac{\partial \gamma_2}{\partial m_1}+\dfrac{Q_2^{-1}}{2c_{0_2}}\dfrac{\partial c_{0_2}}{\partial m_1}\right) & \tilde{\tau}_{p_2}\left(\dfrac{c_{0_2}}{\omega}\dfrac{\partial \gamma_2}{\partial m_2}+\dfrac{Q_2^{-1}}{2c_{0_2}}\dfrac{\partial c_{0_2}}{\partial m_2}\right) & \cdots & (\#2\ mode) \\[2.5ex]
\cdots & \cdots & \cdots & \cdots \\[2.5ex]
\tilde{\tau}_{p_N}\left(\dfrac{c_{0_N}}{\omega}\dfrac{\partial \gamma_N}{\partial m_1}+\dfrac{Q_N^{-1}}{2c_{0_N}}\dfrac{\partial c_{0_N}}{\partial m_1}\right) & \tilde{\tau}_{p_N}\left(\dfrac{c_{0_N}}{\omega}\dfrac{\partial \gamma_N}{\partial m_2}+\dfrac{Q_N^{-1}}{2c_{0_N}}\dfrac{\partial c_{0_N}}{\partial m_2}\right) & \cdots & (\#N\ mode)
\end{bmatrix}_{(N\times k)}
$$

Kernel $\mathbf{G_a}$

The last kernel is $\mathbf{G_a}$. From (GJ.48), we have the relationship between $\mathbf{G_a}$ and Q.

$$
\delta\tau_{\mathbf{a}} = \frac{1}{2}\,\tilde{\tau}_g(\omega)[\,Q^{-1}-\tilde{Q}^{-1}\,] = \mathbf{G_a}\cdot\delta\mathbf{m}
$$

In a manner similar to deriving $\mathbf{G_q}$, we can use the Q and γ relation and the partial derivatives of γ to obtain the kernel $\mathbf{G_a}$ as

$$
(\mathbf{G_a})_n = \frac{\tilde{\tau}_{g_n}(\omega)}{2}\,\frac{\partial Q_n^{-1}}{\partial\mathbf{m}}
$$

$$
= \tilde{\tau}_{g_n}(\omega)\left[\frac{c_{0_n}}{\omega}\frac{\partial\gamma}{\partial\mathbf{m}}+\frac{Q_n^{-1}}{2}\frac{\partial c_{0_n}}{\partial\mathbf{m}}\right]
$$

$\mathbf{G_a}$ in matrix form is

$$
\begin{bmatrix}
\tilde{\tau}_{g_1}\left(\dfrac{c_{0_1}}{\omega}\dfrac{\partial \gamma_1}{\partial m_1}+\dfrac{Q_1^{-1}}{2c_{0_1}}\dfrac{\partial c_{0_1}}{\partial m_1}\right) & \tilde{\tau}_{g_1}\left(\dfrac{c_{0_1}}{\omega}\dfrac{\partial \gamma_1}{\partial m_2}+\dfrac{Q_1^{-1}}{2c_{0_1}}\dfrac{\partial c_{0_1}}{\partial m_2}\right) & \cdots & (\#1\ mode) \\[2.5ex]
\tilde{\tau}_{g_2}\left(\dfrac{c_{0_2}}{\omega}\dfrac{\partial \gamma_2}{\partial m_1}+\dfrac{Q_2^{-1}}{2c_{0_2}}\dfrac{\partial c_{0_2}}{\partial m_1}\right) & \tilde{\tau}_{g_2}\left(\dfrac{c_{0_2}}{\omega}\dfrac{\partial \gamma_2}{\partial m_2}+\dfrac{Q_2^{-1}}{2c_{0_2}}\dfrac{\partial c_{0_2}}{\partial m_2}\right) & \cdots & (\#2\ mode) \\[2.5ex]
\cdots & \cdots & \cdots & \cdots \\[2.5ex]
\tilde{\tau}_{g_N}\left(\dfrac{c_{0_N}}{\omega}\dfrac{\partial \gamma_N}{\partial m_1}+\dfrac{Q_N^{-1}}{2c_{0_N}}\dfrac{\partial c_{0_N}}{\partial m_1}\right) & \tilde{\tau}_{g_N}\left(\dfrac{c_{0_N}}{\omega}\dfrac{\partial \gamma_N}{\partial m_2}+\dfrac{Q_N^{-1}}{2c_{0_N}}\dfrac{\partial c_{0_N}}{\partial m_2}\right) & \cdots & (\#N\ mode)
\end{bmatrix}_{(N\times k)}
$$

Partial Derivatives of c, U, and γ

All four kernels $\mathbf{G_p}$ $\mathbf{G_g}$ $\mathbf{G_q}$ $\mathbf{G_a}$ are derived in terms of partial derivatives of phase velocity c, group velocity U, and attenuation γ. In this section, We will give all partial derivatives which will be used in creating kernels.

Perturbation theory is used to obtain phase velocity partials with respect to medium parameters, and a numerical method which was introduced by Rodi et al.(1975) is used to calculate surface-wave group-velocity partial derivatives. The following equations are calculated for a single mode at a certain frequency, therefore we omit the subscript n for n'th mode. The subscript 0 is used to denote the value before introducing causal Q. The subscript v can be substituted by P-wave velocity α or S-wave velocity β. ρ is layer density. h is layer thickness. ω_r is a reference angular frequency used for introducing causal Q.

Rayleigh Wave

$$c = c_0 + \frac{1}{\pi} \ln(\frac{\omega}{\omega_r}) \sum \left[\frac{\partial c_0}{\partial \beta} \beta Q_\beta^{-1} + \frac{\partial c_0}{\partial \alpha} \alpha Q_\alpha^{-1} \right]$$

$$\gamma = \frac{\omega}{2c_0^2} \sum \left[\frac{\partial c_0}{\partial \beta} \beta Q_\beta^{-1} + \frac{\partial c_0}{\partial \alpha} \alpha Q_\alpha^{-1} \right]$$

$$u = u_0 \left[1 + (2 - \frac{U_0}{c_0})(\frac{c - c_0}{c_0}) + \frac{2\gamma U_0}{\pi \omega} \right]$$

$$\frac{\partial c}{\partial v} = \frac{\partial c_0}{\partial v} \left[1 + \frac{1}{\pi Q_v} \ln(\frac{\omega}{\omega_r}) \right]$$

$$\frac{\partial c}{\partial \rho} = \frac{\partial c_0}{\partial \rho} + \frac{1}{\pi} \ln(\frac{\omega}{\omega_r}) \left[\frac{\partial c_0}{\partial \beta} (-\frac{\beta}{2\rho}) Q_\beta^{-1} + \frac{\partial c_0}{\partial \alpha} (-\frac{\alpha}{2\rho}) Q_\alpha^{-1} \right]$$

$$\frac{\partial c}{\partial h} = \frac{\partial c_0}{\partial h}$$

$$\frac{\partial c}{\partial Q_v^{-1}} = \frac{1}{\pi} \ln(\frac{\omega}{\omega_r}) \frac{\partial c_0}{\partial v} v$$

$$\frac{\partial \gamma}{\partial v} = \frac{\omega}{2c_0^2} \frac{\partial c_0}{\partial v} Q_v^{-1} - \frac{2\gamma}{c_0} \frac{\partial c_0}{\partial v}$$

$$\frac{\partial \gamma}{\partial \rho} = \frac{\omega}{2c_0^2} \left[\frac{\partial c_0}{\partial \beta} (-\frac{\beta}{2\rho}) Q_\beta^{-1} + \frac{\partial c_0}{\partial \alpha} (-\frac{\alpha}{2\rho}) Q_\alpha^{-1} \right] - \frac{2\gamma}{c_0} \frac{\partial c_0}{\partial \rho}$$

$$\frac{\partial \gamma}{\partial h} = -\frac{2\gamma}{c_0} \frac{\partial c_0}{\partial h}$$

$$\frac{\partial \gamma}{\partial Q_v^{-1}} = \frac{\omega}{2c_0^2} \frac{\partial c_0}{\partial v} v$$

$$\frac{\partial U}{\partial v} = \frac{\partial U_0}{\partial v} \left[\frac{U}{U_0} - \frac{U_0}{c_0} (\frac{c-c_0}{c_0}) + \frac{2\gamma U_0}{\pi \omega} \right] + \frac{\partial c_0}{\partial v} (\frac{U_0}{c_0})^2 \left[2\frac{c}{c_0} - 2\frac{c}{U_0} - 1 \right]$$

$$+ \frac{\partial c}{\partial v} \frac{U_0}{c_0} (2 - \frac{U_0}{c_0}) + \frac{\partial \gamma}{\partial v} \frac{2u_0^2}{\pi \omega}$$

$$\frac{\partial U}{\partial \rho} = \frac{\partial U_0}{\partial \rho} \left[\frac{U}{U_0} - \frac{U_0}{c_0} (\frac{c-c_0}{c_0}) + \frac{2\gamma U_0}{\pi \omega} \right] + \frac{\partial c_0}{\partial \rho} (\frac{U_0}{c_0})^2 \left[2\frac{c}{c_0} - 2\frac{c}{U_0} - 1 \right]$$

$$+ \frac{\partial c}{\partial \rho} \frac{U_0}{c_0} (2 - \frac{U_0}{c_0}) + \frac{\partial \gamma}{\partial \rho} \frac{2u_0^2}{\pi \omega}$$

$$\frac{\partial U}{\partial h} = \frac{\partial U_0}{\partial h} \left[\frac{U}{U_0} - \frac{U_0}{c_0} (\frac{c-c_0}{c_0}) + \frac{2\gamma U_0}{\pi \omega} \right] + \frac{\partial c_0}{\partial h} (\frac{U_0}{c_0})^2 \left[2\frac{c}{c_0} - 2\frac{c}{U_0} - 1 \right]$$

$$+ \frac{\partial c}{\partial h} \frac{U_0}{c_0} (2 - \frac{U_0}{c_0}) + \frac{\partial \gamma}{\partial h} \frac{2u_0^2}{\pi \omega}$$

$$\frac{\partial U}{\partial Q_v^{-1}} = \frac{U_0}{c_0} (2 - \frac{U_0}{c_0}) \frac{\partial c}{\partial Q_v^{-1}} + \frac{2u_0^2}{\pi \omega} \frac{\partial \gamma}{\partial Q_v^{-1}}$$

14

Love Wave

$$c = c_0 + \frac{1}{\pi} \ln(\frac{\omega}{\omega_r}) \sum \frac{\partial c_0}{\partial \beta} \beta Q_\beta^{-1}$$

$$\gamma = \frac{\omega}{2c_0^2} \sum \frac{\partial c_0}{\partial \beta} \beta Q_\beta^{-1}$$

$$u = u_0 \left[1 + (2 - \frac{U_0}{c_0})(\frac{c - c_0}{c_0}) + \frac{2\gamma U_0}{\pi \omega} \right]$$

$$\frac{\partial c}{\partial \beta} = \frac{\partial c_0}{\partial \beta} \left[1 + \frac{1}{\pi Q_v} \ln(\frac{\omega}{\omega_r}) \right]$$

$$\frac{\partial c}{\partial \rho} = \frac{\partial c_0}{\partial \rho} + \frac{1}{\pi} \ln(\frac{\omega}{\omega_r}) \left[\frac{\partial c_0}{\partial \beta} (-\frac{\beta}{2\rho}) Q_\beta^{-1} \right]$$

$$\frac{\partial c}{\partial h} = \frac{\partial c_0}{\partial h}$$

$$\frac{\partial c}{\partial Q_\beta} = \frac{1}{\pi} \ln(\frac{\omega}{\omega_r}) \frac{\partial c_0}{\partial \beta} \beta$$

$$\frac{\partial \gamma}{\partial \beta} = \frac{\omega}{2c_0^2} \frac{\partial c_0}{\partial \beta} Q_\beta^{-1} - \frac{2\gamma}{c_0} \frac{\partial c_0}{\partial \beta}$$

$$\frac{\partial \gamma}{\partial \rho} = \frac{\omega}{2c_0^2} \left[\frac{\partial c_0}{\partial \beta} (-\frac{\beta}{2\rho}) Q_\beta^{-1} - \frac{2\gamma}{c_0} \frac{\partial c_0}{\partial \rho} \right]$$

$$\frac{\partial \gamma}{\partial h} = -\frac{2\gamma}{c_0} \frac{\partial c_0}{\partial h}$$

$$\frac{\partial \gamma}{\partial Q_\beta^{-1}} = \frac{\omega}{2c_0^2} \frac{\partial c_0}{\partial \beta} \beta$$

$$\frac{\partial U}{\partial \beta} = \frac{\partial U_0}{\partial \beta} \left[\frac{U}{U_0} - \frac{U_0}{c_0} (\frac{c - c_0}{c_0}) + \frac{2\gamma U_0}{\pi \omega} \right] + \frac{\partial c_0}{\partial \beta} (\frac{U_0}{c_0})^2 \left[2\frac{c}{c_0} - 2\frac{c}{U_0} - 1 \right]$$

$$+ \frac{\partial c}{\partial \beta} \frac{U_0}{c_0} (2 - \frac{U_0}{c_0}) + \frac{\partial \gamma}{\partial \beta} \frac{2u_0^2}{\pi \omega}$$

$$\frac{\partial U}{\partial \rho} = \frac{\partial U_0}{\partial \rho} \left[\frac{U}{U_0} - \frac{U_0}{c_0} (\frac{c - c_0}{c_0}) + \frac{2\gamma U_0}{\pi \omega} \right] + \frac{\partial c_0}{\partial \rho} (\frac{U_0}{c_0})^2 \left[2 \frac{c}{c_0} - 2 \frac{c}{U_0} - 1 \right]$$

$$+ \frac{\partial c}{\partial \rho} \frac{U_0}{c_0} (2 - \frac{U_0}{c_0}) + \frac{\partial \gamma}{\partial \rho} \frac{2u_0^2}{\pi \omega}$$

$$\frac{\partial U}{\partial h} = \frac{\partial U_0}{\partial h} \left[\frac{U}{U_0} - \frac{U_0}{c_0} (\frac{c - c_0}{c_0}) + \frac{2\gamma U_0}{\pi \omega} \right] + \frac{\partial c_0}{\partial h} (\frac{U_0}{c_0})^2 \left[2 \frac{c}{c_0} - 2 \frac{c}{U_0} - 1 \right]$$

$$+ \frac{\partial c}{\partial h} \frac{U_0}{c_0} (2 - \frac{U_0}{c_0}) + \frac{\partial \gamma}{\partial h} \frac{2u_0^2}{\pi \omega}$$

$$\frac{\partial U}{\partial Q_\beta^{-1}} = \frac{U_0}{c_0} (2 - \frac{U_0}{c_0}) \frac{\partial c}{\partial Q_\beta^{-1}} + \frac{2u_0^2}{\pi \omega} \frac{\partial \gamma}{\partial Q_\beta^{-1}}$$

4. Forming Inversion Kernel

As shown above, we calculate partial derivatives with respect to all parameters (α, β, ρ, Q_α, Q_β, h) instead of computing partial derivatives for shear velocity only. The intention is that we try to provide all the possible tools to interpret the seismograms as completely as possible, and as automatically as possible. Therefore, it is the users' responsibility to choose those model parameters they want to invert; and only the chosen part will be used to assemble the inversion kernel.

To stabilize the inversion, all information for different frequencies inside the inversion kernel are weighted according to their frequency amplitudes. This weighting procedure greatly improves the inversion stability.

When inverting teleseismic surface-waveforms, sometimes the body waves (e.g. *SS*, *SSS*) or some unwanted surface-waves due to improper rotation will have bad influence on the cross_correlation between the isolation function and the observed seismogram, and cause signal misalignment. To avoid this problem, a window is applied on the seismograms before doing cross-correlation, and this may successfully isolate the surface wave

wavetrain from those body waves outside the surface wave wavetrain. Although prewindowing procedure is applied, the same trouble still may happen occasionally. In such a situation, the information at that frequency must be rejected from forming inversion kernel, otherwise it will plague the inversion for its strong misaligned "phase delay" or "group delay". Figure 1 shows an example of this problem. Due to improper rotation, the unwanted Love-wave waveform appears on the radial component seismogram prior to the Rayleigh wave wavetrain. This unwanted Love wave signal causes two kinds of mistakes, wrong identification of a Gaussian wavelet (Figure 1a) and signal misalignment (Figure 1b), which can not be incorporated in inversion.
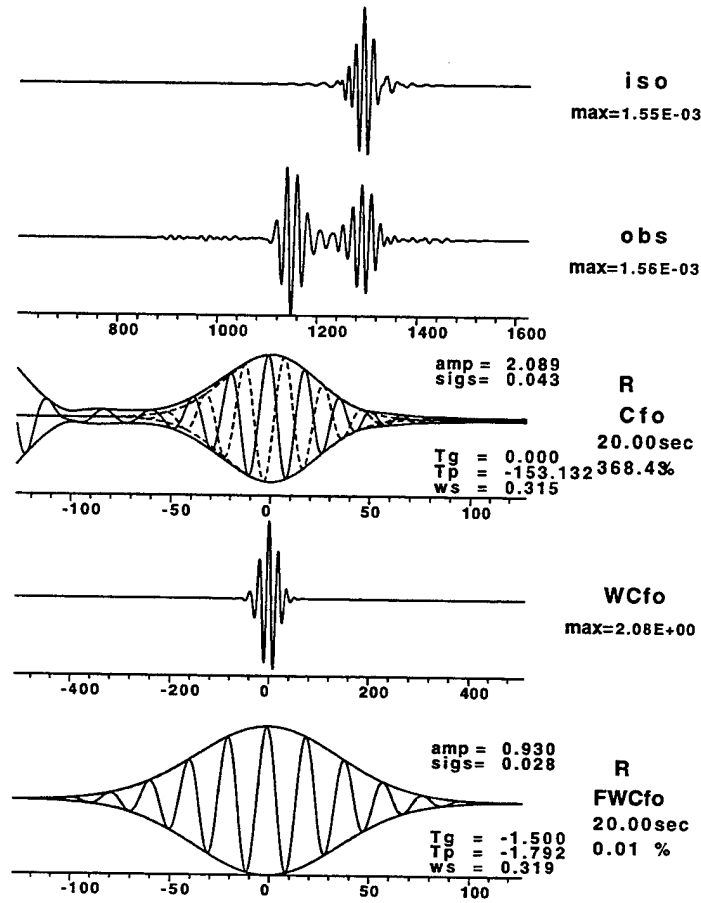
Figure 1. This is an example showning how unexpected signal interference affects the extracting procedure in GSDF theory. There are five traces presented to show the different processing stages. The top two traces are the prefiltered isolation filter and observed seismogram, respectively, The third trace shows the Gaussian filtered cross-correlation at a target period of 20.0 seconds. The five extracted parameters are shown. The dashed curves inside the envelope are from the synthetics and the solid curve are from the observed data. The fourth trace is the windowed cross-correlagram shown in the third trace. The bottom trace is the filtered windowed cross-correlagram and its five Gaussian wavelet parameters which are to be used in further processing. Due to improper rotation, the Love wave appears on radial component before the Rayleigh wave arrival. The Love wave wavetrain may causes two kind troubles like (a) wrong determination of Gaussian wavelet parameters, and

We have mentioned that users have the power to decide what parameters will be inverted for during the inversion. An aspect which strongly related to this decision is the phrase "using what kind information ?". During each iteration in the inversion, we have calculated partial derivatives with respect to parameters for each layer at several appointed frequencies, and all this information is rearranged to form four kind delays at each frequency. After manually rejecting miscalculated cross_correlations at some

18

iso
max=8.81E-04

obs
max=1.56E-03

800   1000   1200   1400   1600

amp = 4.468
sigs= 0.038   **R**

                     Cfo

                     25.00sec
Tg = -145.000
Tp = -131.660 10.86%
ws = 0.282

-250   -200   -150   -100   -50

WCfo
max=4.44E+00

-400   -200   0   200   400

amp = 1.686
sigs= 0.023   **R**

                     FWCfo
                     25.00sec
Tg = -144.500
Tp = -130.071 0.06 %
ws = 0.258
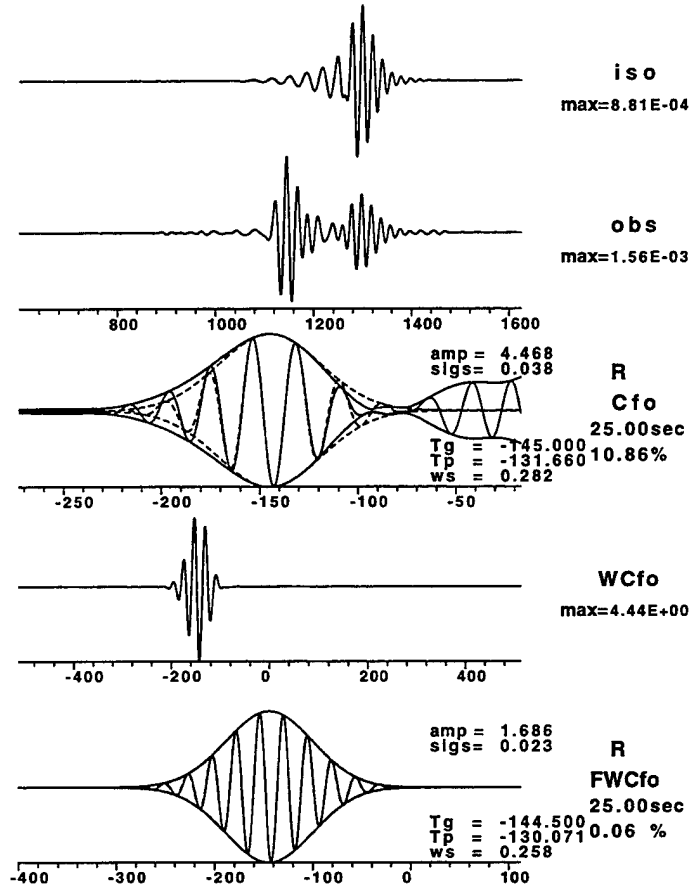
-400   -300   -200   -100   0   100

Figure 1. (cont'd). (b) Misalignment of signals which produces significant bias phase and group delay. This arises because a period of 25 seconds is considered compared to 20 seconds in Figure 1a.

frequencies, users have to decide which combinations of δt_p, δt_g, δt_a, δt_q they will use to invert for a particular combination of model parameters (α, β, ρ, Q_α, Q_β, h). From our experience, we found that when we invert for velocity structure the phase delay (δt_p) and the group delay (δt_g) play the major roles in inversion, and the other two delays (δt_a, δt_q) are better in inverting for attenuation factors. We also found that when the initial model is far from the final result, using group delay information in inversion can easily pull the model close enough to the final model so that phase delays can be used. It is only at the final stage when the synthetic is very close to the observed seismograms that the phase delay information can be used at a powerful fine tuning of the model since there is no "cycle skipping" problem.

5. Synthetic Test

A simple source with strike, dip, rake angles of 45°, 45°, 45°, respectively, in 20 km deep was used in this synthetic test. Receiver is located at 1000 km away along 10° in azimuth. The "observed" seismograms were created for a two layered crust with an upper mantle deviating slightly from the PREM model (Figure 2). Here, we only try to invert for shear velocity structure, so all the other parameters related to the source and earth model are assumed known. The starting model is a two-layered crust model with the PREM model beneath 40 km depth. It is clearly seen in Figure 3 that the starting synthetic seismograms are very far away "observed" seismograms.
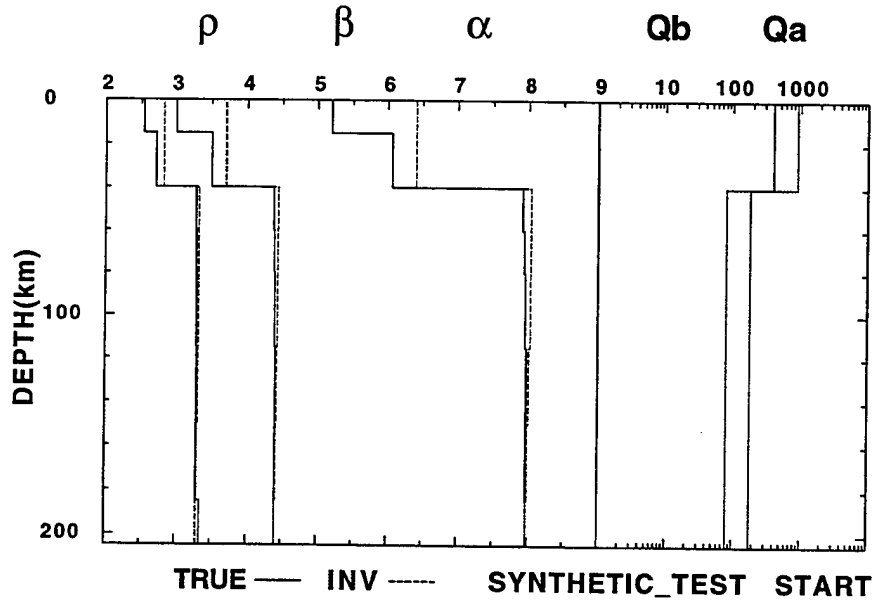

Figure 2. The starting model (dashed line) used in synthetic test of GSDF inversion algorithm and the "true" model (solid line) used to create the "observed data".

After 12 iterations, the synthetic seismograms are almost the same as "observed" seismograms (Figure 4). Checking the model differences between the "true" model and the final model (Figure 5), we can see the crust structure almost matches the "true" model, except in the upper mantle where the surface wave doesn't provide enough resolving power and the inverted structure is causing the "zig-zag" pattern. The differences in Q models are not significant at these frequencies and this distance.

20

SYNTHETIC_TEST   START VEL

Z
obs.Z
4.888E-04
syn.Z
2.509E-04

R
obs.R
3.654E-04
syn.R
1.714E-04

T
obs.T
5.302E-04
syn.T
2.904E-04

FILTER   Flo=0.010   Fhi=0.050 (Hz) Norder= 4

LON=0.000   LAT=0.000   DEPTH= 20.00
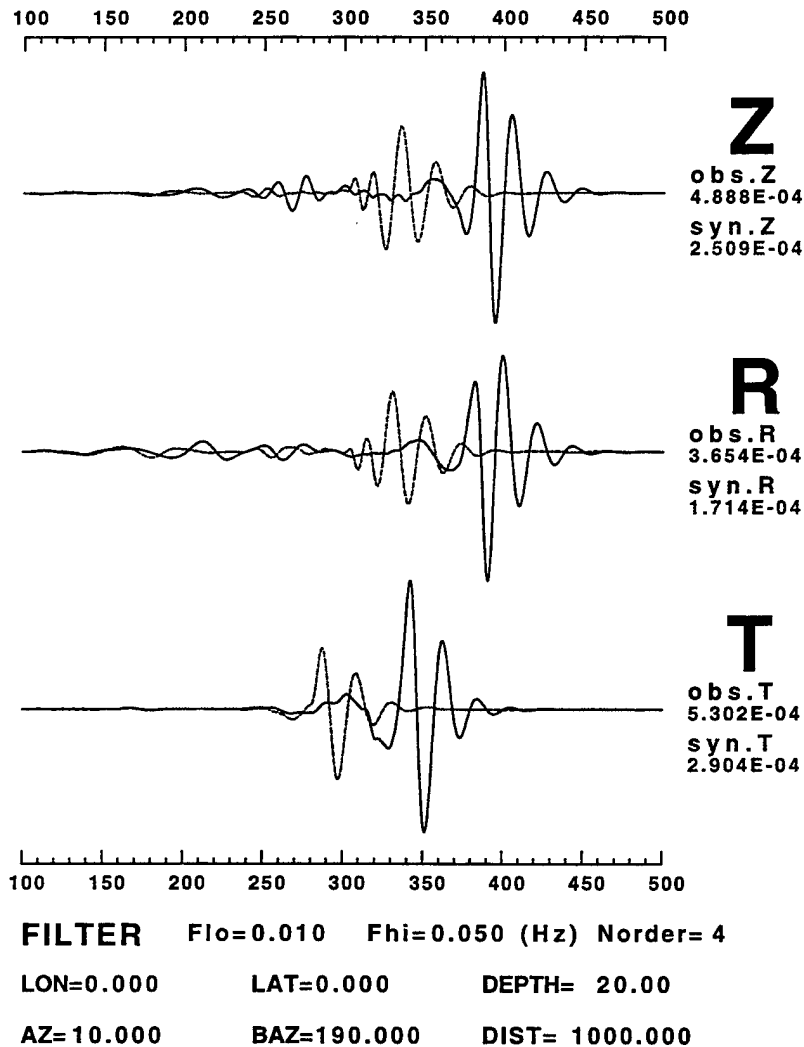
AZ=10.000   BAZ=190.000   DIST= 1000.000

Figure 3. The velocity time histories of "observed seismograms" (solid line) and the those from the starting model (dashed line) are both filtered in the frequency band 0.01-0.05 Hz by using a Butterworth filter with four poles. The plotted seismograms are normalized according the maximum amplitude of each component in current frequency band. It is clear to see that the starting model is not close to the "true" model and this may demonstrate the ability of the inversion programs to resolve structure.

6. Real Data Test

After the successful synthetic test, we wish to test this technique on real data. The April 14, 1995 Texas earthquake is the one chosen. According to Sipkin's USGS solution, the epicenter of the Texas earthquake is at 30.261°N
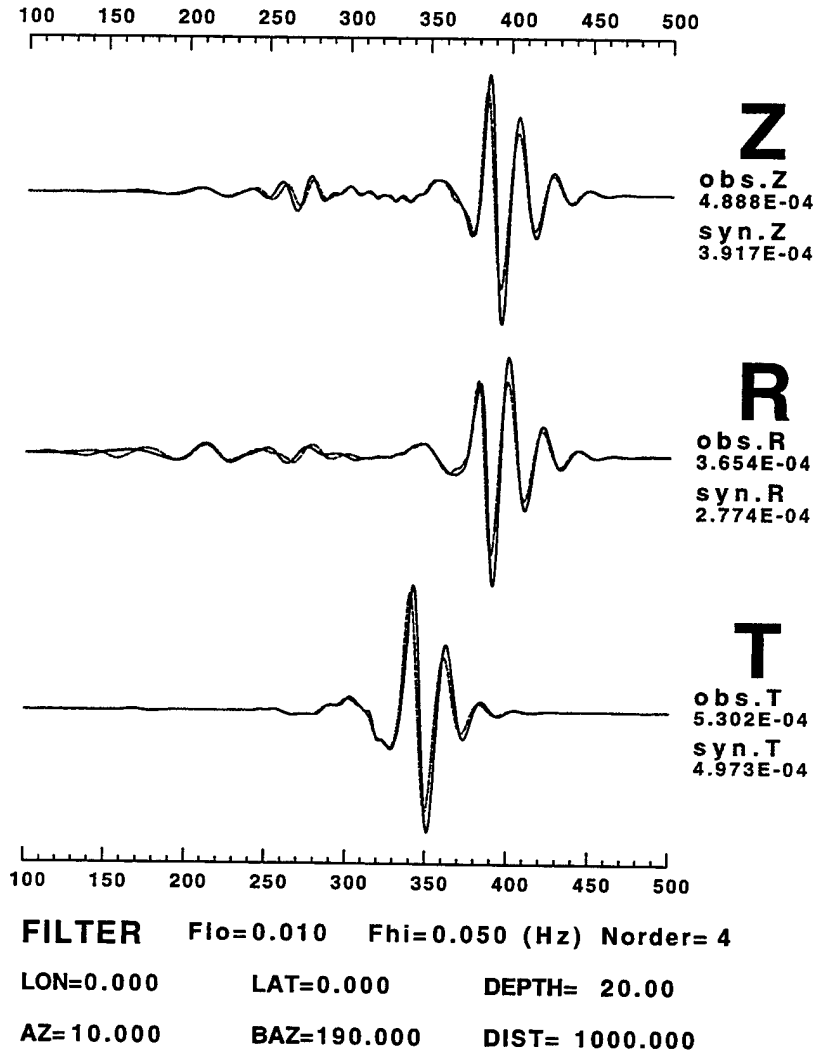
SYNTHETIC_TEST   FINAL   VEL

Figure 4. After 12 iterations, the final inversion result show an predicted waveforms almost identical to the "observed seismograms".

103.33°W and origin time is 00:32:55UT. The current collected data set consists of 49 broadband stations from IRIS, Canadian National Seismological Center (CNSDC), USGS, and UNAM (Figure 6).

Some source parameters were redetermined on the basis of fitting surface wave amplitude spectra. The redetermined source depth is 23 km deep, with strike, dip, rake angles of 114°, 64°, -101°, respectively with M_w = 5.6. From some stations whose epicenter distances greater than 3600 km, it is
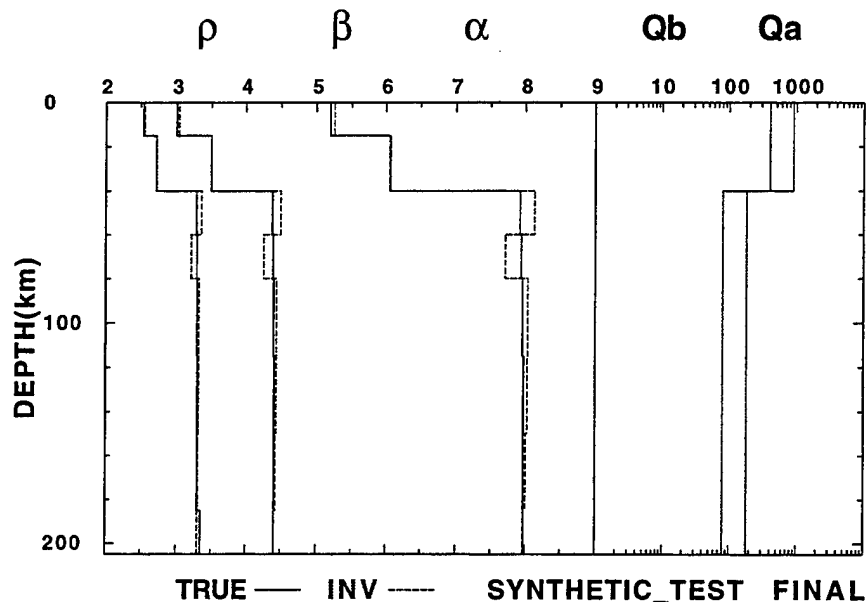
Figure 5. The comparison between the final model and the "true model". We can see that the 2-layer crust is very close to the "true" model, but that in the upper mantle the model shows some "zig-zag" pattern.

easy to see a systematically 7-9 seconds travel time difference between pP and P arrivals (Figure 7). This observation confirms that the source depth is deeper than those suggested by USGS Sipkin's solution (13 km) and Harvard's CMT solution (15 km).

The focal mechanism generally matches the surface wave amplitude spectra radiation pattern at periods 5-60 seconds (Figures 8a and 8b). The source time function used in this study is a parabolic source time function with 2.0 seconds duration.

7. Inversion Procedure

We have tried three different inversion runs, the first two exhibit some significant difficulties in matching the waveform or in reasonableness of the resulting model, so the third one has been adapted for inverting structure. In performing the inversions, we use an earth flattening approximation to use plane-layered surface-wave theory to generate synthetics.

The first run consisted of a joint inversion of both Rayleigh and Love wave seismograms for shear velocity structure. The result was that the
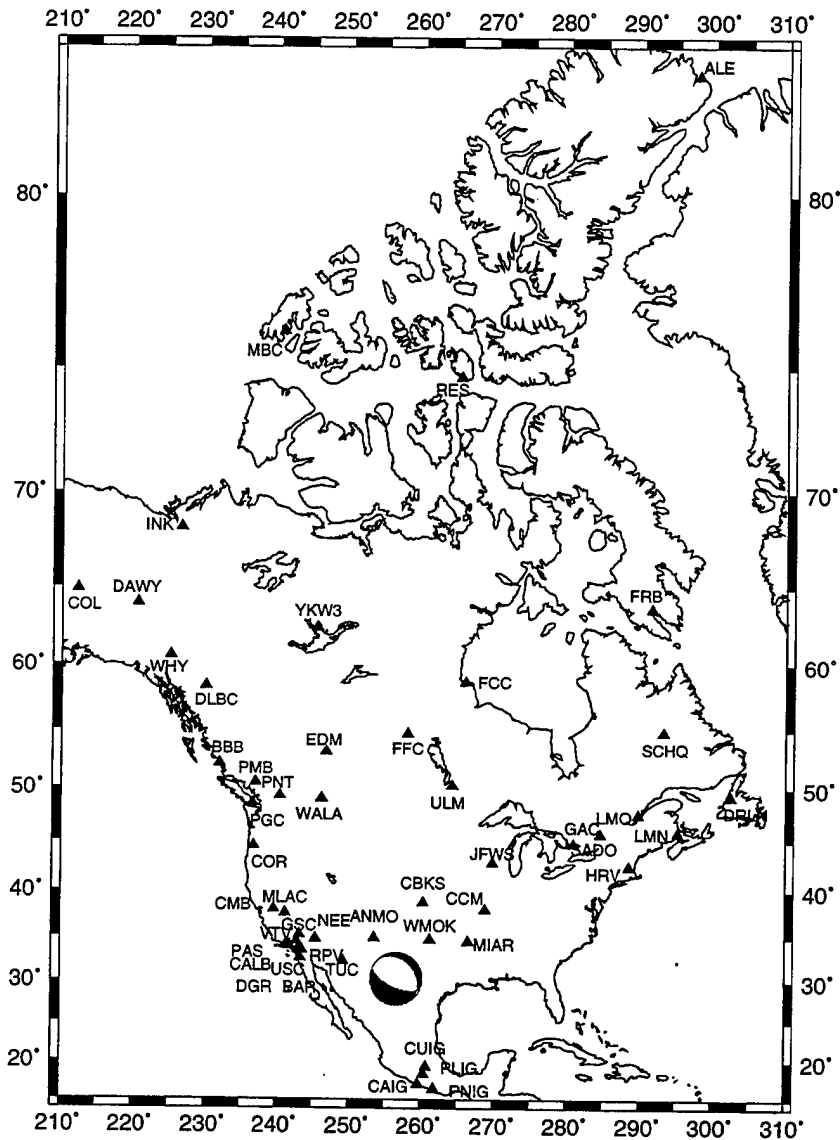
Figure 6. The Texas earthquake in relation to stations providing broadband data.

synthetic seismograms tended to fit the largest surface wave amplitude, and ignored the small amplitude wavefields. This arose because of the amplitude level weighting used to stabilize the inversion. Therefore, separate inversions for Rayleigh wave and Love wave were necessary.

The second sequence consisted of inverting for the shear velocity structure from the Love wave, and then using this structure as an *a priori* shear
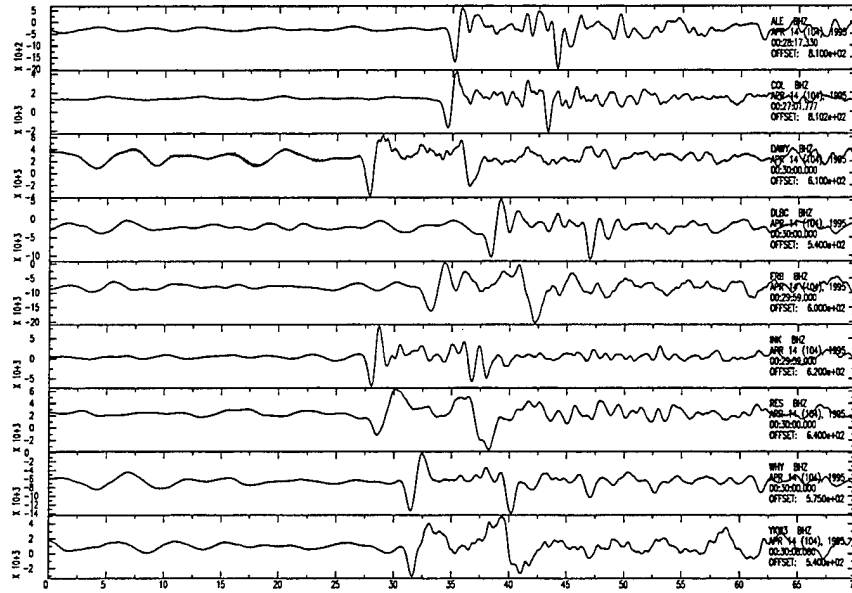
24

Figure 7. Nine stations whose epicentral distance greater than 3600 km show a general 7-9 seconds in differential travel time between pP and P phase. This supports a source depth deeper than 20 km.

velocity structure so the the Rayleigh wave provided information on the compressional velocity structure. This procedure can match both Rayleigh wave and Love wave waveforms very well, but we found it is impossible to find a reasonable explanation for the anomalous Poisson's ratios in the inverted model. It is well known that the surface waves are insensitive to compressional wave velocity structure, so the only conclusion for this is that the shear velocity structure inverted from Love wave is not adequate for Rayleigh wave. An unaccounted anisotropy effect may cause the overcorrection in compression velocity structure. Figure 9 compares waveforms and Figure 10, shows the model resulting from the second inversion procedure. Although the synthetic waveform does not perfectly fit the Rayleigh wave (Figure 9), we can see the general features are matched using a single model for both Love and Rayleigh waves. In Figure 10 we see that the P-wave velocity structure has lower values to compensate for the high shear velocity, and vice versa. The results are some unexplainable Poisson's ratios such as 0.135
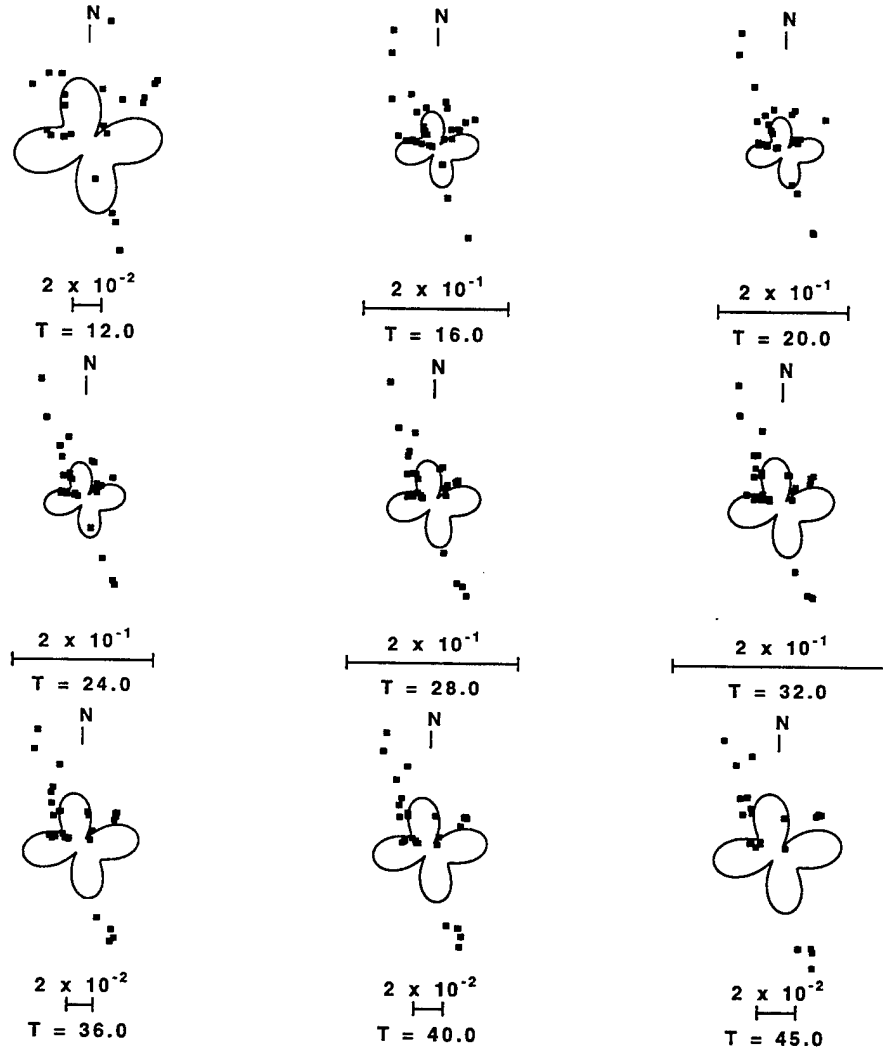
25

Figure 8. The source mechanism is redeterminated by fitting the surface wave amplitude spectra radiation pattern at periods 5-60 seconds. (a). The Love wave radiation pattern for the preferred solution. The bars indicate attenuation corrected spectral amplitudes in cm-sec normalized for geometrical spreading to 1000 km.

for the middle crust and 0.328 for the lower crust.

Since our forward synthetic seismogram algorithm does not include anisotropy effect, we modify our inversion procedure as as follows: we invert V_{β_SH} from Love wave, and another separate inversion of V_{β_PSV} from Rayleigh wave on the vertical component. We fixed the Poisson's ratio when we invert V_{β_PSV} from Rayleigh wave. The fixed Poisson's ratios are kept the same as the original input model. In this study, we set the Poisson's ratio as 0.25 for crust, 0.28 for the layers between 40 km and 220 km, and adopt the
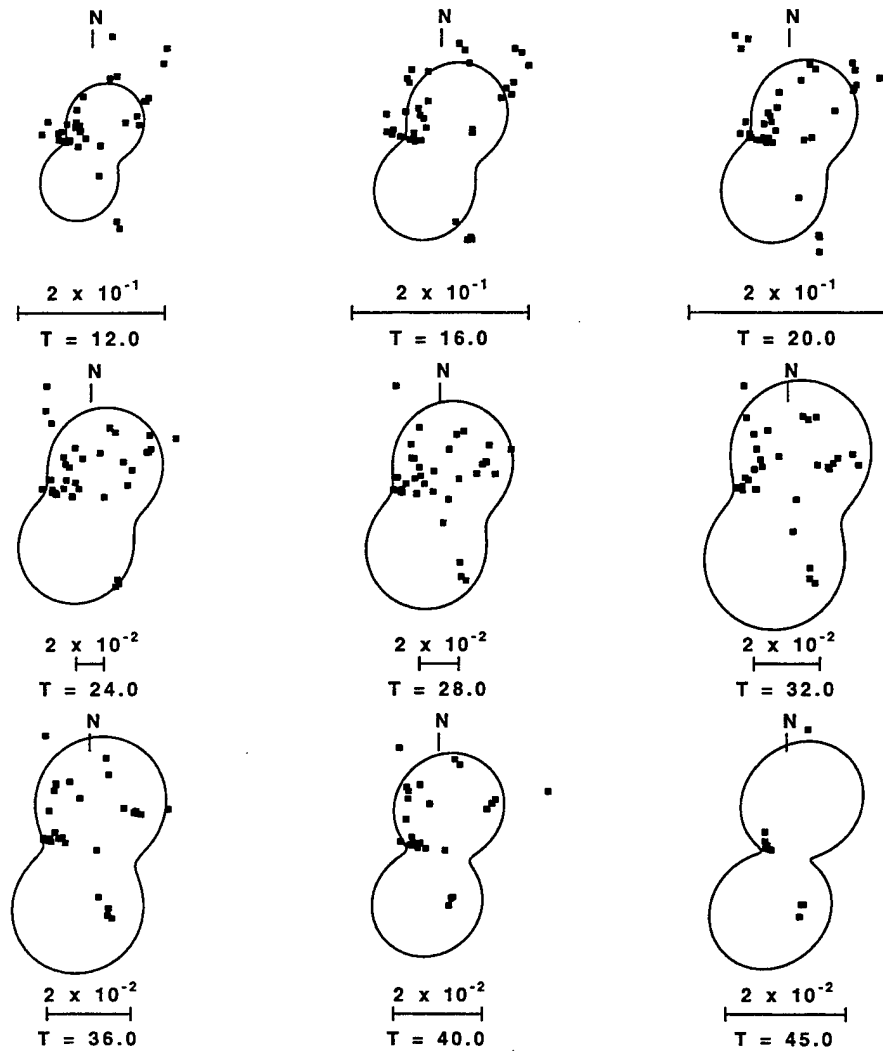
Figure 8. (Cont'd). (b) Comparison of observed and predicted Rayleigh wave radiation patterns.
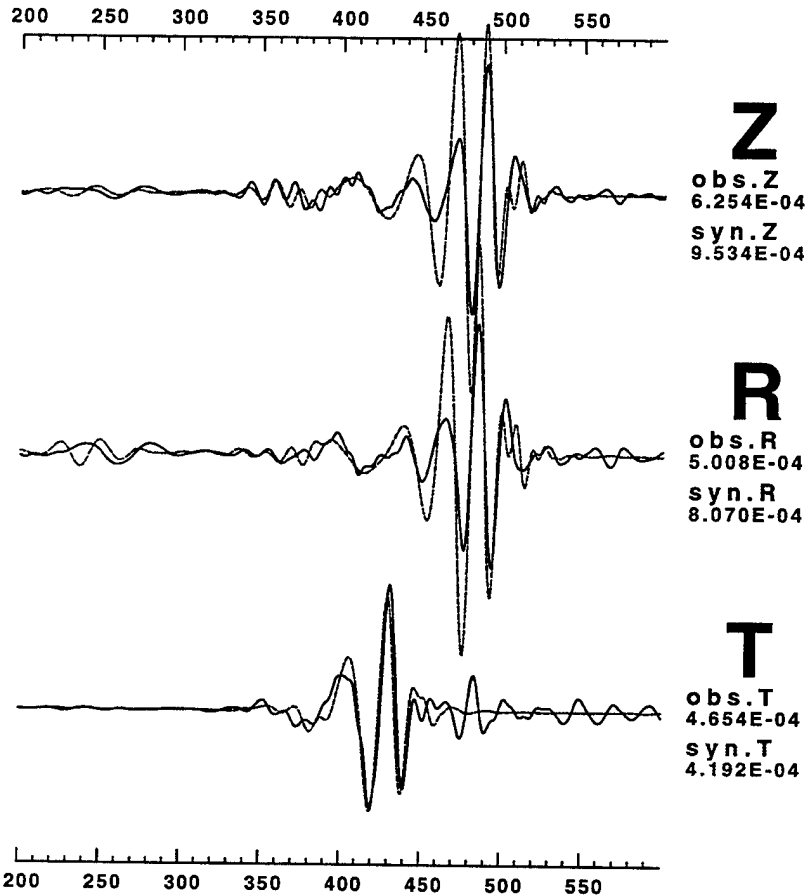
values from PREM model for those layers deeper than 220 km.

When we invert for shear-wave velocity structures, the attenuation factors can be determined simultaneous either by joint inversion of V_β and Q or by another separated Q inversion. The Q determination is not definitive, since we have a lot uncertainties in our source and velocity structures in our inversion, so the only objective criteria for determining Q is the envelope shape of the surface wave wavetrain. As shown on Figure 11, the Rayleigh wave signal at large distance is well dispersed with a strong Airy phase. This Airy phase corresponding is affected by crustal wave propagation, therefore,

TEXAS950414   **CCM**   VEL

Z
obs.Z
6.254E-04
syn.Z
9.534E-04

R
obs.R
5.008E-04
syn.R
8.070E-04

T
obs.T
4.654E-04
syn.T
4.192E-04

FILTER   Flo=0.010   Fhi=0.050 (Hz) Norder= 4

LON=-103.327   LAT=30.261   DEPTH= 23.00

AZ=48.918   BAZ=235.704   DIST= 1408.160

Figure 9. The result of inversion using the second procedure. This inversion procedure inverts S wave velocity from Love wave and after that inverts P wave velocity from Rayleigh wave by assuming no anisotropy effect. This shows a acceptable waveform match in phase, but not in envelope.

the envelope amplitude of the Airy phase is controlled by the crustal attenuation factors. So the Q structure determined is sensitive to the crust and uppermost mantle.
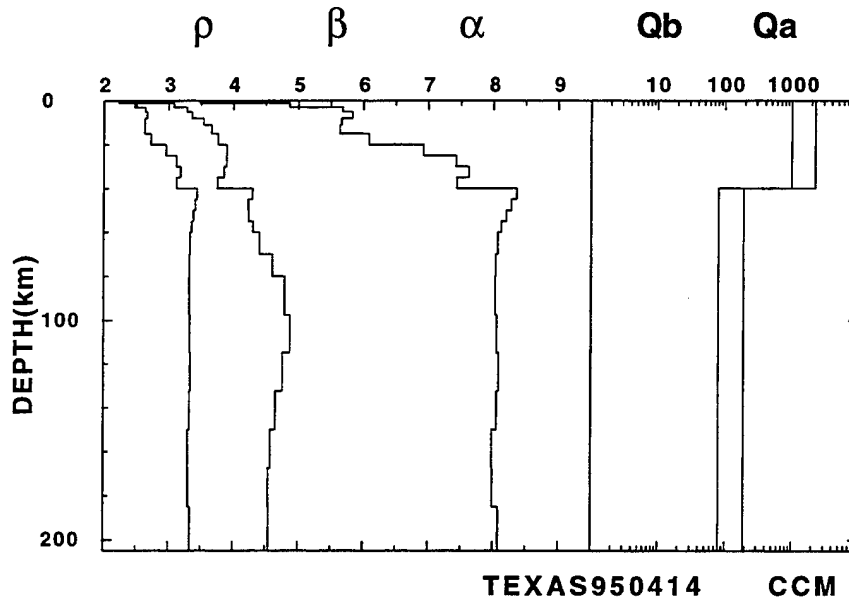
Figure 10. The model inverted by the second inversion procedure.

8. Inversion results

Data from 43 of 49 broadband stations were inverted. In this report, three stations were selected to present the inversion results and the waveform fitting success will be shown on several different frequency bands.

Station ALE, which located in Arctic region is the farthest station used in this study. There are some interesting features for the inverted results. Looking at the waveform fit in the low frequency range (0.005-0.03 Hz bandpass; shown as Figure 11a), it is clear to see that the synthetic seismograms successfully match the observed surface wave. Two velocity models, PSV and SH are inverted respectively from Rayleigh wave and Love wave.

For ALE, the attenuation factor was fixed during inversion. A high Q structure ($Q_S = 1000$) is used for crust, a low Q ($Q_S = 100$) was adopted for structure between 40 km and 500 km, and using $Q_S = 143$ for those deeper than 220 km. And from Figures 11a,b, the synthetic Rayleigh wave and Love wave amplitudes only show small deviation from observed seismogram, therefore the Q model is considered adequate. We also notice this sharp Q contrast between crust and mantle is a common character for those stations located inside the North America craton region.

TEXAS950414   ALE   DISP

Z
obs.Z
1.698E-04
syn.Z
1.168E-04

R
obs.R
1.650E-04
syn.R
1.281E-04

T
obs.T
1.489E-04
syn.T
1.297E-04

FILTER   Flo=0.005   Fhi=0.030 (Hz) Norder= 4

LON=-103.327   LAT=30.261   DEPTH= 23.00
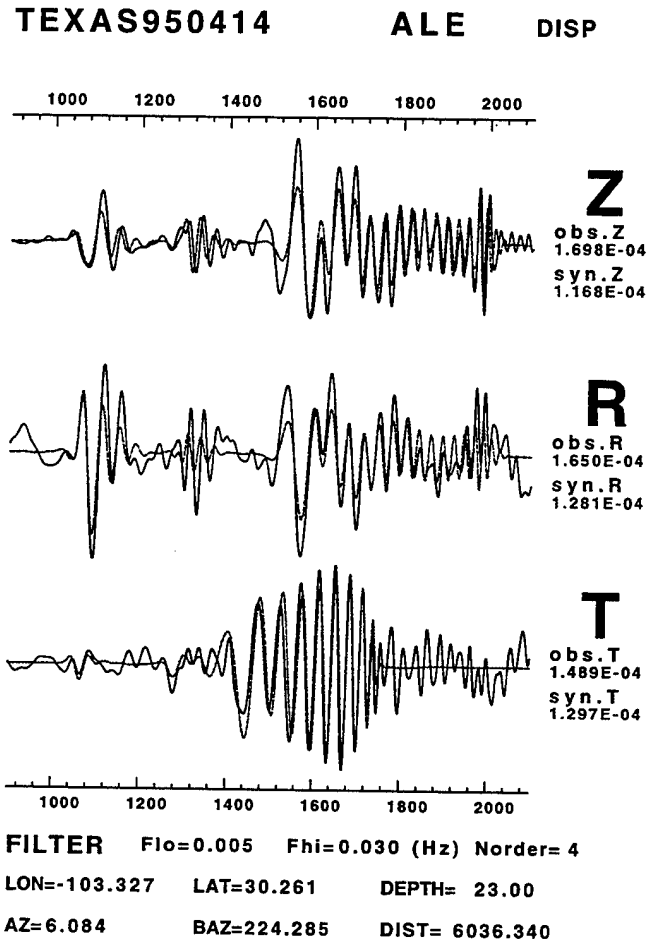
AZ=6.084   BAZ=224.285   DIST= 6036.340

Figure 11a. Waveform fit of the final inverted model for ALE in the frequency band of 0.005-0.03 Hz. The signal which arrives at 1020 seconds and around 1300 seconds are S and SS phase, respectively. From the S phase waveform, we can say that the source time function used in this inversion is a little short but is close enough.

The second station is FCC which located on the west shoreline of Hudson Bay and is in the center of the North America craton. The inverted models (Figure 13) show high shear velocity for upper mantle but not as high as SNA model (Grand and Helmberger, 1984). The current inversion result shows 4.5% anisotropy between 70 km and 140 km. The synthetics fit data well at low frequency (Figure 14a) and can fit the fundamental mode as high as 0.1 Hz (Figure 14), but have difficulty to produce some higher mode arrivals at 800 and 940. the time range.

The final station is PAS. The wave propagates through the southern Rocky Mountains. The inverted model (Figure 15) does not require

TEXAS950414 **ALE** DISP

FILTER   Flo=0.005   Fhi=0.050 (Hz) Norder= 4

LON=-103.327   LAT=30.261   DEPTH= 23.00
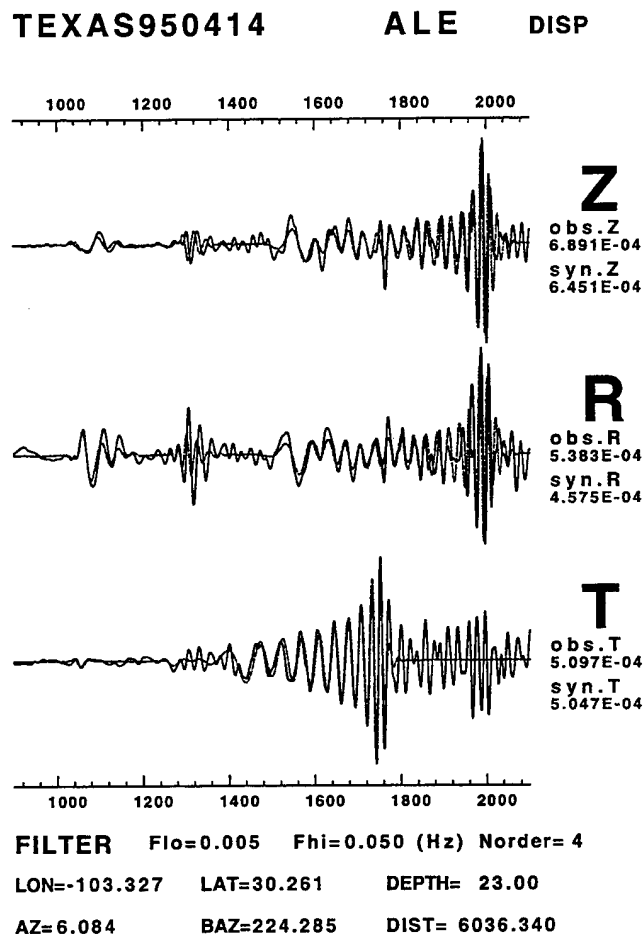
AZ=6.084   BAZ=224.285   DIST= 6036.340

Figure 11b. (Cont'd). Waveform fit in the 0.005-0.05 Hz frequency band.

anisotropy and the shear velocity model is very close to the TNA model (Grand and Helmberger, 1984). The synthetics fit the S phase which arrives around 350 seconds and surface wave very well (Figures 16abc) and this suggests that there is a velocity discontinuity at 220 km which can not be seen in the TNA model. The Q is very low, with the average Q for crust of lower than 200. However we found one interesting feature about the Q behavior. The Q values between 40 and 220 km are slightly higher than PREM model, i.e., a low Q crust underlain a slightly high Q upper mantle with respect to the ref-
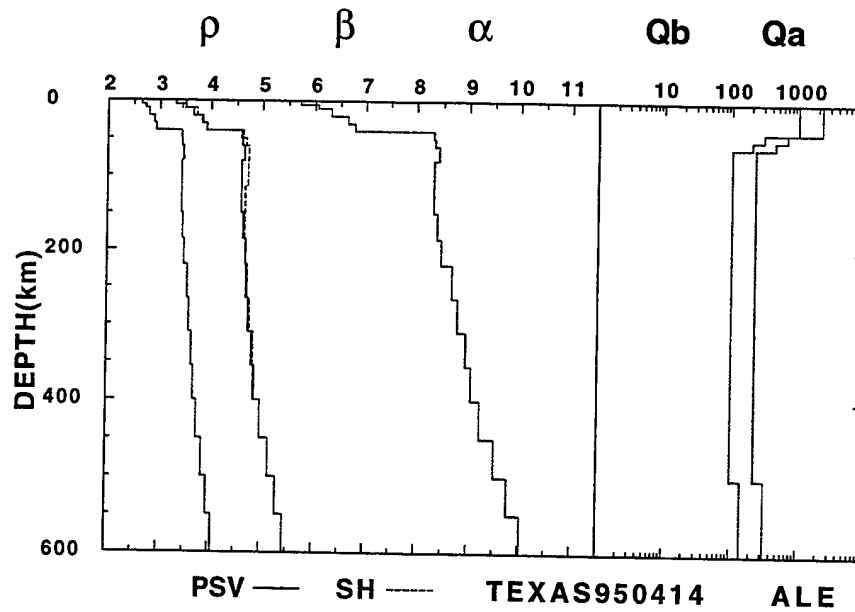
Figure 12. The inverted models for ALE. Two models (PSV and SH) were inverted for Love wave and Rayleigh Wave. From these two models, there is one slight anisotropic zone above 200 km.
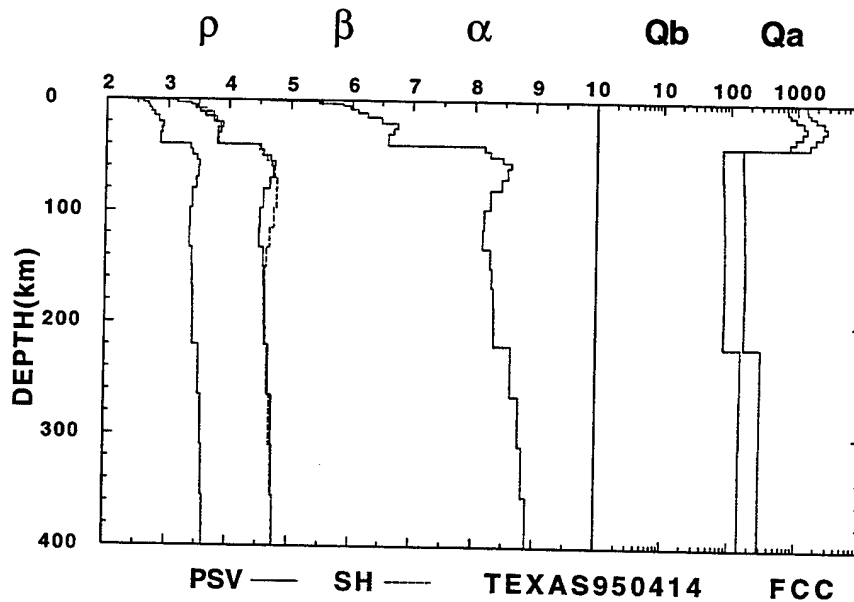

Figure 13. The final inverted model for FCC. There is 4.5% anisotropy effect exists between 70 and 140 km.

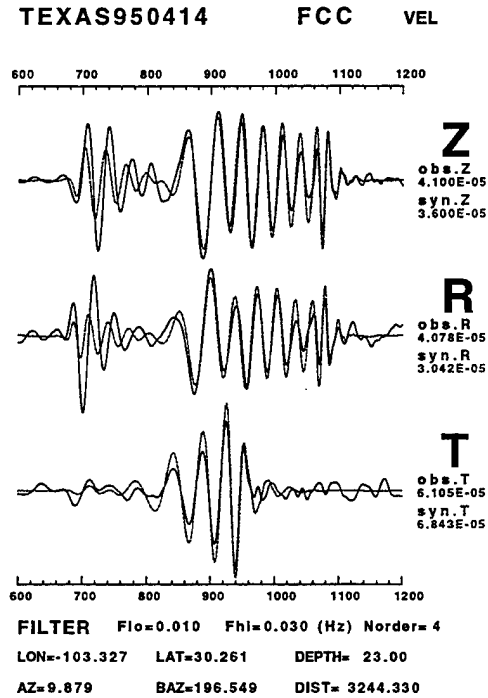erence model.

TEXAS950414   FCC   VEL

Figure 14. The waveform fitting for final model in FCC are shown at three frequency bands :
(a) 0.01-0.03 (b) 0.01-0.05 (c) 0.01-0.1 Hz. The SS phase arrives at 660 seconds. The inverted
model can fit fundamental mode Love wave and Rayleigh wave waveforms as high as 0.1 Hz,
but it lacks the ability to simulate the higher modes.

9. Conclusion

We implemented the Generalized Seismological Data Functionals tech-
nique of Gee and Jordan (1992) in a surface-wave waveform inversion algo-
rithm. A simple synthetic test shows its robust inversion ability. After a suc-
cessful synthetic test, we useed this inversion algorithm on real data to fur-
ther test its ability. The Texas earthquake (30.26 °N 103.33°W, 00:32:55UT,
April 14, 1995) is a very good earthquake for this purpose because it was well
recorded, its source depth is well constrained, the focal mechanism is fairly
determined, and the seismic moment is constrained by long period surface
waves. The inversion results are excellent and show some interesting fea-
tures. For the craton there is some evidence for anisotropy and crustal Q is
high. For the mountain region, although the inverted model show very simi-
lar shear velocity structure like TNA model, but from the S-wave waveform
the model prefers a velocity discontinuity at 220 km. These features worth
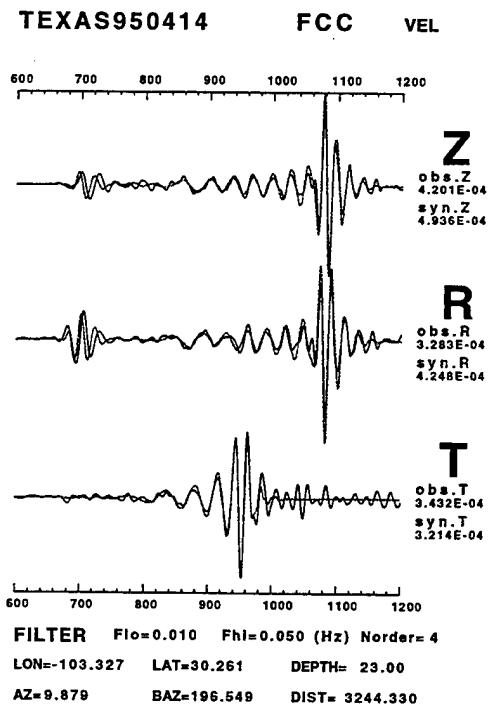more effect on them.

TEXAS950414   FCC   VEL

Figure 14. (Cont'd). (b) 0.01-0.05 Hz.

10. References

Gee, L. S. & Jordan, T. H., 1992. Generalized seismological data functionals, *Geophys. J. Int.,* **111,** 363-390.

Rodi, W. L., Glover, P., Li, T. M. C. & Alexander, S. S., 1975. A fast, accurate method for computing group-velocity partial derivatives for Rayleigh and Love modes. *Bull. Seism. Soc. Am.,* **65,** 1105-1114.

TEXAS950414   **FCC**   VEL

FILTER   Flo=0.010   Fhi=0.100 (Hz) Norder= 4

LON=-103.327   LAT=30.261   DEPTH= 23.00

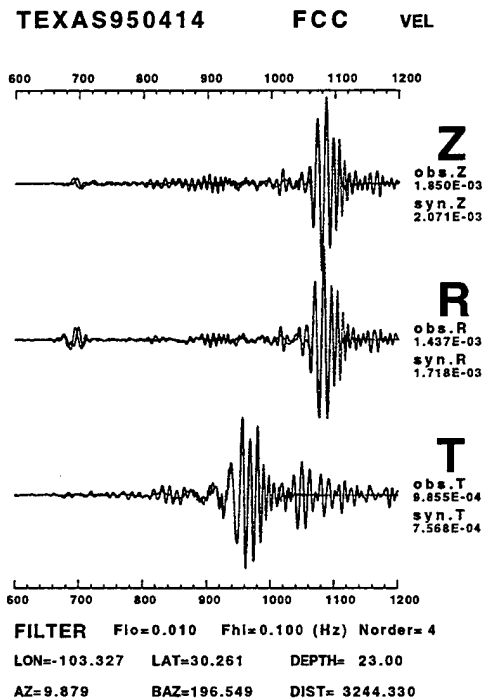AZ=9.879   BAZ=196.549   DIST= 3244.330

Figure 14. (Cont'd). (c) 0.01-0.1 Hz. The SS phase arrives at 660 seconds. The inverted model can fit fundamental mode Love wave and Rayleigh wave waveforms as high as 0.1 Hz, but it lacks the ability to simulate the higher modes.
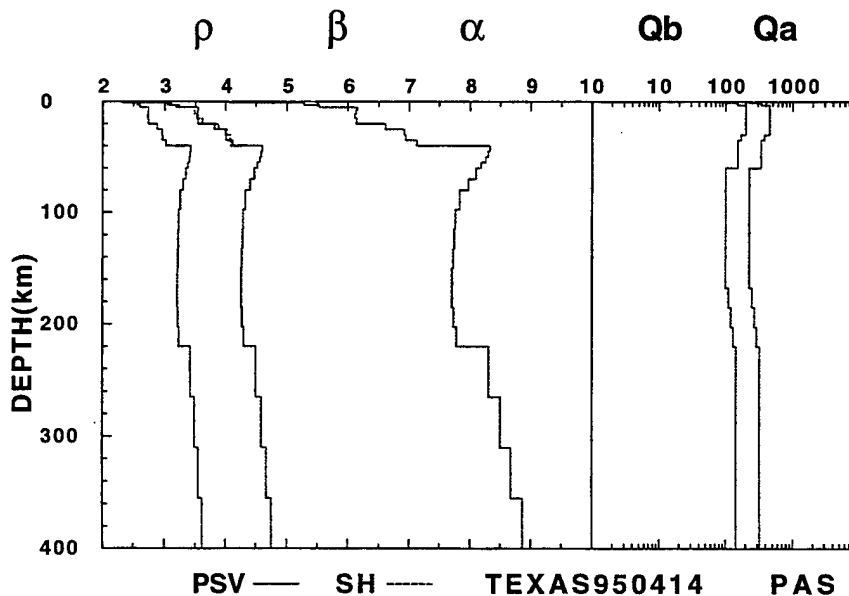

Figure 15. The inverted models for PAS. There is no clear anisotropy effects. The crustal Q is very low.
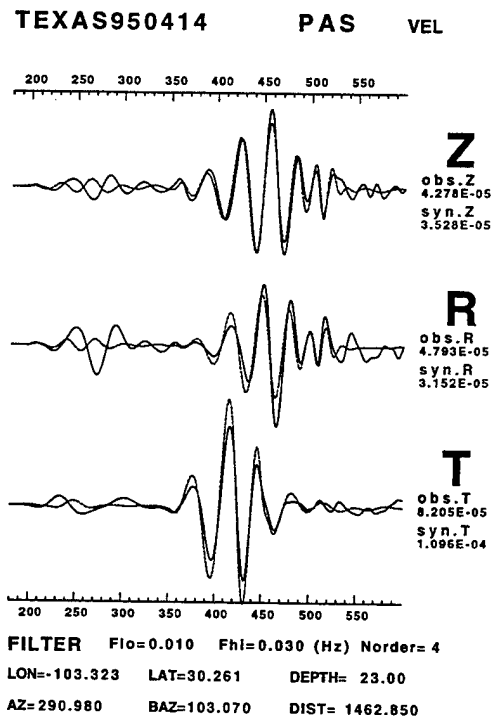
Figure 16. Waveform fitting are shown on three frequency bands : (a) 0.01-0.03 (b) 0.01-0.05 and (c) 0.01-0.1 Hz. The S wave signal arrives at 350 seconds.
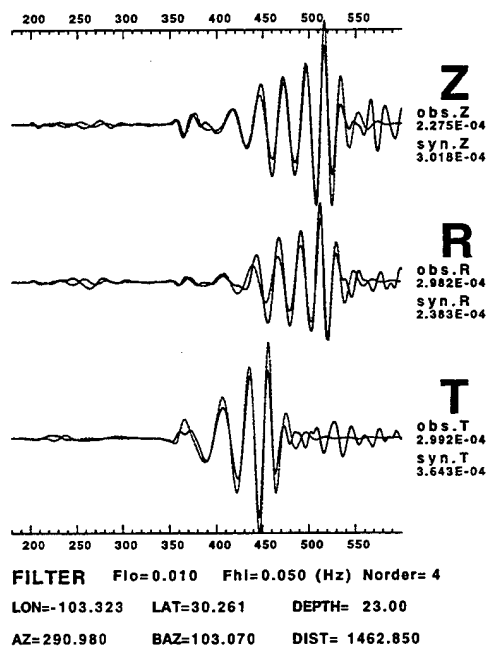
TEXAS950414   PAS   VEL

200   250   300   350   400   450   500   550

Z
obs.Z
2.275E-04
syn.Z
3.018E-04

R
obs.R
2.982E-04
syn.R
2.383E-04

T
obs.T
2.992E-04
syn.T
3.643E-04

200   250   300   350   400   450   500   550

FILTER   Flo=0.010   Fhl=0.050 (Hz) Norder= 4

LON=-103.323   LAT=30.261   DEPTH= 23.00

AZ=290.980   BAZ=103.070   DIST= 1462.850

Figure 16. (Cont'd). (b) 0.01-0.05 Hz.

TEXAS950414   PAS   VEL

200   250   300   350   400   450   500   550

Z
obs.Z
9.089E-04
syn.Z
1.261E-03

R
obs.R
1.464E-03
syn.R
1.069E-03

T
obs.T
7.111E-04
syn.T
1.035E-03

200   250   300   350   400   450   500   550

FILTER   Flo=0.010   Fhl=0.100 (Hz) Norder= 4

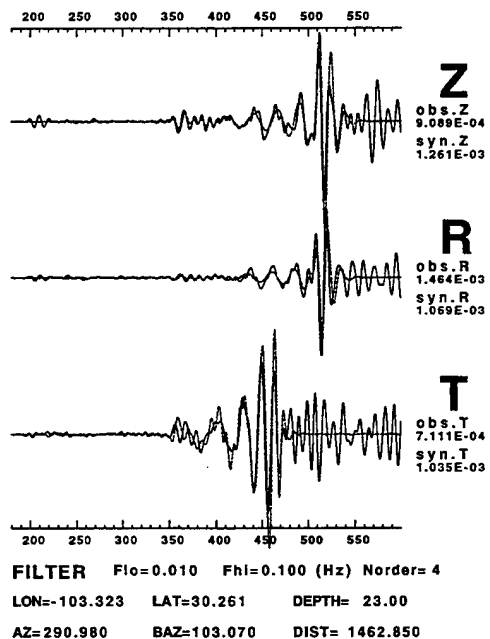LON=-103.323   LAT=30.261   DEPTH= 23.00

AZ=290.980   BAZ=103.070   DIST= 1462.850

Figure 16. (Cont'd). (c) 0.01-0.1 Hz.